Models for the active site of oxygen-binding hemoproteins. Dioxygen binding properties and the structures of (2-methylimidazole)-meso-tetra(α,α,α,α-o pivalamidophenyl)porphyrinatoi...

ARTICLE *in* JOURNAL OF THE AMERICAN CHEMICAL SOCIETY · APRIL 1980

Impact Factor: 12.11 · DOI: 10.1021/ja00529a055

7 AUTHORS, INCLUDING:

Geoffrey B Jameson
Massey University
254 PUBLICATIONS **5,286** CITATIONS
SEE PROFILE

Eric Rose
Pierre and Marie Curie University - Paris 6
188 PUBLICATIONS **3,507** CITATIONS
SEE PROFILE

the reactions (Scott, R. A., unpublished results).
(29) Yu, C.-A.; Yu, L. *Biochem. Biophys. Res. Commun.* **1976**, *70*, 1115.
(30) Gilmour, M. V.; Wilson, D. F.; Lemberg, R. *Biochim. Biophys. Acta* **1967**, *143*, 487.
(31) However, we emphasize at this time that one such reasonable alternative is a simple bimolecular mechanism involving electron transfer from $Ru(NH_3)_6^{2+}$ to a^{3+}.
(32) The intermolecular redox process could also involve a reduced copper site as the primary electron donor to a_3^{3+} ($a^{2+}a_3^{3+}$(red Cu) + $a^{2+}a_3^{3+} \rightarrow$ (k_{slow}) $a^{2+}a_3^{3+}$(ox Cu) + $a^{2+}a_3^{2+}$). Additional experiments will be required terpretations of the second-order dependence of the slow phase are also possible. One such interpretation is that the deviation of the slow phase from (pseudo-)first-order behavior is due to the presence of two first-order decays with similar (but not identical) rate constants. However, the excellent second-order fits place severe restrictions on the relative values of such rate constants; and, for this reason, the second-order interpretation is preferred.
(33) Wherland, S.; Gray, H. B. "Biological Aspects of Inorganic Chemistry", Addison, A. W., Cullen, W., James, B. R., Dolphin, D., Eds.; Wiley: New York, 1977; p 289.
(34) Holwerda, R. A.; Wherland, S.; Gray, H. B. *Annu. Rev. Biophys. Bioeng.* **1976**, *5*, 363.

Models for the Active Site of Oxygen-Binding Hemoproteins. Dioxygen Binding Properties and the Structures of (2-Methylimidazole)-*meso*-tetra($\alpha,\alpha,\alpha,\alpha$-*o*-pivalamidophenyl)porphyrinatoiron(II)–Ethanol and Its Dioxygen Adduct

Geoffrey B. Jameson,[1a] Frank S. Molinaro,[1a] James A. Ibers,*[1a] James P. Collman,*[1b] John I. Brauman,[1b] Eric Rose,[1b] and Kenneth S. Suslick[1b,c]

Contribution from the Departments of Chemistry, Northwestern University, Evanston, Illinois 60201, Stanford University, Stanford, California 94305, and University of Illinois, Urbana, Illinois 61801. *Received August 1, 1979*

Abstract: When crystals of (2-methylimidazole)-*meso*-tetra($\alpha,\alpha,\alpha,\alpha$-*o*-pivalamidophenyl)porphyrinatoiron(II)-ethanol, Fe(TpivPP)(2-MeIm)·EtOH, are exposed to dioxygen, the crystals of the resultant dioxygen adduct are still suitable for diffraction studies. The direct, precise determination of the stereochemical changes accompanying oxygenation of an iron(II)-(porphyrinato)(base) complex has been carried out using conventional X-ray diffraction methods. The structures have been refined by full-matrix, least-squares methods, using 4176 and 5183 reflections for the deoxy and oxy complexes, respectively, to R indices on F^2 of 0.162 and 0.120. For the portion of data where $F_o^2 > 3\sigma(F_o^2)$ the respective indices on F are 0.086 and 0.083. Crystal data for the deoxy compound follow: space group C_{2h}^6-$C2/c$, $Z = 4$, molecular symmetry C_2, $a = 18.871$ (11) Å, $b = 19.425$ (13) Å, $c = 18.434$ (11) Å, $\beta = 91.48$ (3)°, $V = 6755.0$ Å^3. The oxy complex is nearly isomorphic with $Z = 4$ in space group $C2/c$ with a cell of dimensions $a = 18.864$ (5) Å, $b = 19.451$ (5) Å, $c = 18.287$ (5) Å, $\beta = 91.45$ (2)°, $V = 6707.0$ Å^3. Some selected parameters for the coordination spheres, with those in square brackets pertaining to the dioxygen adduct, follow: Fe-N_{porph} = 2.068 (5), 2.075 (5) [1.997 (4), 1.995 (4)] Å; Fe-N_{Im} = 2.095 (6) [2.107 (4)] Å. The iron atom is displaced 0.399 [0.086] Å from the least-squares plane of the porphinato nitrogen atoms toward the imidazole ligand. The Fe-O separation is 1.898 (7) Å. The average O-O separation is 1.22 (2) Å and the Fe-O-O angle is 129 (1)°. In the presence of ethanol the deoxy complex binds dioxygen reversibly, noncooperatively, and with lower affinity than when the sample is desolvated—in the latter case dioxygen uptake has been found to be cooperative. The structure and properties of these possible models for T-state deoxy- and oxyhemoglobin are correlated and then compared with the 1-methylimidazole analogue. The sterically active 2-methyl substituent appears to perturb the Fe-O bond but not the Fe-N_{Im} bond.

Introduction

The structural changes which occur at the heme center upon the binding of dioxygen, carbon monoxide, nitric oxide, and alkyl isocyanides to hemoglobins, normal and abnormal, are of great importance to an understanding of structure-function relationships. In particular, discussions on the mechanism of cooperativity in the binding of small molecules to hemoglobin have been strongly influenced by structural data and physical measurements obtained from simple model systems;[2-8] this influence is manifested in the evolving concepts of Perutz.[9,10] In the absence of precise data from protein crystal structures, an absence that arises not from faults in the experiment but is intrinsic in the nature of the problem, model complexes have been invaluable as a means of establishing the general geometry of small molecule-hemoglobin complexes[11-15] and of understanding some general structure-function relationships.

Complexes of Fe(TPP)(1-MeIm)[16] with small molecules (O_2, CO, and NO) can be taken as models for the corresponding myoglobin adducts or for hemoglobin in the R (or high ligand affinity) states as the binding properties of the base, 1-methylimidazole, closely resemble those of the biological axial base, histidine. The recent studies of abnormal hemoglobins, with either unusually high or low ligand affinities,[17] are of considerable use in understanding the behavior of normal hemoglobins. It is often difficult to find appropriate model analogues. But by adding a sterically active substituent to the axial base, such as exists in 2-methylimidazole,[4b,18,19] or by creating steric strain in a covalent chain linking an imidazole base to the porphyrin skeleton,[20] affinities for small molecules are reduced. These systems at least mimic if not model low-affinity hemoglobins or T-state hemoglobin.[5,18,20,21] A very close structural correspondence between such model compounds and the metal sites of oxygen-binding hemoproteins has been established using techniques such as Mössbauer,[22-24] extended X-ray absorption fine structure (EXAFS),[6] resonance Raman spectroscopy,[25,26] and infrared spectroscopy.[27,28]

0002-7863/80/1502-3224$01.00/0

Table I. Crystal Data and Data Collection Procedures for Fe(TpivPP)(2-MeIm)·EtOH (I) and Fe(O_2)(TpivPP)(2-MeIm)·EtOH (II)

	I	II
formula	$FeC_{70}N_{10}O_5H_{76}$	$FeC_{70}N_{10}O_7H_{76}$
formula wt	1193.30 amu	1225.30 amu
space group	C_{2h}^6-$C2/c$	C_{2h}^5-$C2/c$
a	18.871(12) Å	18.864(5) Å
b	19.425(13) Å	19.451(5) Å
c	18.434(11) Å	18.287(5) Å
β	91.48(3)°	91.45(2)°
V	6755.0 Å^3	6707.7 Å^3
Z	4	4
ρ_{obsd}, ρ_{calcd}	1.19(2), 1.17 g cm^{-3}	−, 1.21 g cm^{-3}
temp	21 °C	21 °C
crystal shape	needle, 0.21 × 0.29 × 0.71 mm	needle, 0.27 × 0.29 × 0.75 mm
crystal vol	0.042 mm^3	0.046 mm^3
radiation	graphite-monochromated Mo Kα, λ(Kα$_1$) = 0.7093 Å	Ni-filtered, Cu Kα, λ(Kα$_1$) = 1.540 562 Å
linear absorption coeff	2.73 cm^{-1}	22.6 cm^{-1}
transmission factors	0.92–0.96[a]	0.44–0.62
detector aperture	5.1 mm wide, 5.3 mm high 32 cm from crystal	5.2 mm wide, 6.0 mm high 32 cm from crystal
take-off angle	2.8°	4.2°
scan speed	2.0° in 2θ per min	2.0° in 2θ per min
λ^{-1} sin θ limits	0.0554–0.5281 4.5 < 2θ(Mo Kα) < 44.0°	0.0198–0.5691 3.5 < 2θ(Cu Kα) < 122.5°
background counts	initially 10 s, then 20 s at each end of scan with rescan option[b]	similar to I
scan range	0.8° below Kα$_1$, 0.8° above Kα$_2$	0.9° below Kα$_1$, 0.9° above Kα$_2$
data collected	±h, k, l	±h, k, l
p	0.04	0.05
unique data	4176	5183
unique data with $F_o^2 > 3\sigma(F_o^2)$	2263	3086

[a] No absorption correction applied for I. [b] Lenhert, P. G. *J. Appl. Crystallogr.* **1975**, *8*, 568–570.

Using the compounds Fe(TpivPP)(2-MeIm)·EtOH (I) and Fe(O_2)(TpivPP)(2-MeIm)·EtOH (II), we may probe quantitatively the structural changes which could occur upon oxygenation of T-state hemoglobin to give T-state oxyhemoglobin. Furthermore, this pair of structures provides a unique opportunity to relate changes in geometry to ligand binding properties in a situation where the crystal packing influences remain very similar. We have already communicated the salient features of these structures.[29] Here we provide a more complete description and discussion of our results.

Experimental Section

Preparation of Compounds. The deoxy compound, Fe(TpivPP)(2-MeIm)·EtOH (I), was prepared as described in ref 18. Crystals suitable for single-crystal X-ray diffractometry were obtained by recrystallization from refluxing ethanol, and were sealed under dry dinitrogen gas in thin-walled, quartz capillaries. The dioxygen adduct, Fe(O_2)(TpivPP)(2-MeIm)·EtOH (II), was prepared by exposing crystals of I for 3 days at 20 °C to 1–2 atm of dioxygen gas which was saturated with ethanol vapor. Crystals were then rapidly sealed in capillaries.

Crystallographic Data for I. Precession and Weissenberg photographs displayed symmetry and systematic absences consistent with the monoclinic space groups C_{2h}^6-$C2/c$ or C_s^4-Cc. Diffraction data were collected on a Picker FACS-I automatic diffractometer with graphite-monochromated Mo Kα radiation. Lattice parameters were obtained as previously described[29] by hand centering 14 reflections in the range $0.2169 < \lambda^{-1} \sin\theta < 0.2581$ Å^{-1} using Mo Kα$_1$ radiation (λ = 0.7093 Å). Crystal data and details of data collection are summarized in Table I.

Crystallographic Data for II. Formation of the dioxygen adduct was not accompanied by loss of crystallinity. With respect to I, no changes in symmetry or systematic absences and only small changes in unit cell constants were observable, although there were many significant changes in intensities of non-$h0l$ reflections. Identical behavior was observed for all crystals of II which were tested (more than five). Except where stated explicitly, experimental conditions similar to those for I prevailed. Data were collected in this instance with Ni-prefiltered Cu Kα radiation. Crystal mosaicities (peak width at half peak height for ω scans) ranged from 0.20 to 0.30°; some reflections had a minor shoulder. Lattice parameters were derived from the setting angles of 16 reflections in the range $0.1952 < \lambda^{-1} \sin\theta < 0.2912$ Å^{-1} (Cu Kα$_1$, λ = 1.540 562 Å).

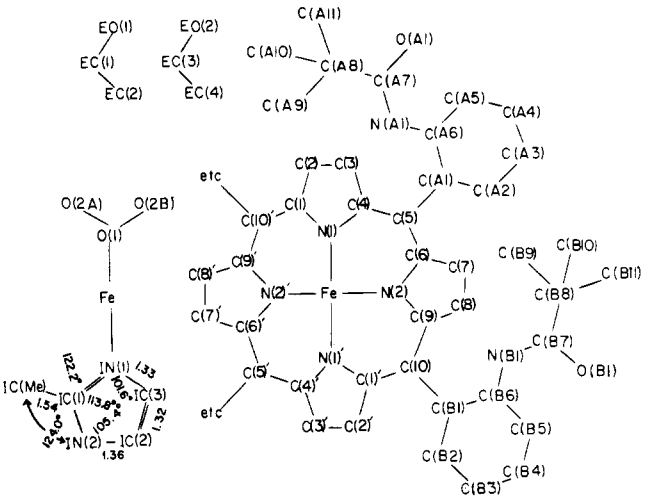

Figure 1. Atom labeling scheme for Fe(TpivPP)(2-MeIm)·EtOH.

Solution and Refinement of Structure I. The usual procedures, computer programs, atomic scattering factors, and anomalous dispersion terms were employed.[13,30] In the initial development and refinement of the structure, the Northwestern University CDC6600 computer was used. In the final cycles of refinement the Lawrence Berkeley Laboratory CDC7600 computer was accessed by remote telephone connection.

Space group $C2/c$ was assumed; consequently twofold symmetry is imposed on the molecular species. Subsequent successful refinement of the structure in this space group, negligible differences in the intensities of 544 Friedel pairs, and the failure of refinements in the alternative space group Cc to yield a better defined model justified the initial assumption. Since the solution and refinement of both this

Table II. Final Atomic Parameters for Fe(TpivPP)(2-MeIm)·EtOH

ATOM	X[A]	Y	Z	B11[B]	B22	B33	B12	B13	B23
FE	0	0.117341(78)	1/4	29.71(51)	36.70(55)	24.70(50)	0	-1.86(37)	0
N(1)	0.09845(28)	0.13764(27)	0.20811(27)	30.7(20)	39.2(23)	22.8(20)	-1.7(16)	-0.8(16)	2.0(16)
C(1)	0.11534(36)	0.13754(35)	0.13548(37)	32.0(27)	38.6(30)	27.6(26)	-0.1(21)	3.9(21)	-0.8(21)
C(2)	0.19066(40)	0.14210(39)	0.12936(40)	37.5(30)	45.6(33)	35.5(31)	2.7(24)	7.1(24)	3.0(24)
C(3)	0.21943(36)	0.14537(38)	0.19707(39)	31.1(26)	47.9(33)	32.4(29)	-4.8(22)	2.5(23)	1.1(24)
C(4)	0.16182(37)	0.14249(34)	0.24601(38)	31.9(26)	36.4(28)	31.4(27)	-1.0(21)	0.1(22)	2.0(22)
C(5)	0.16925(37)	0.14290(34)	0.32209(38)	32.5(26)	32.0(27)	33.1(28)	0.2(20)	-3.5(22)	-2.1(21)
N(2)	0.04346(27)	0.13814(26)	0.35221(27)	30.7(21)	36.6(23)	21.5(19)	-3.6(16)	-1.3(16)	-1.6(16)
C(6)	0.11358(37)	0.14100(34)	0.37106(36)	30.6(26)	35.7(28)	27.0(26)	-0.2(21)	-4.6(21)	-2.7(20)
C(7)	0.12241(39)	0.14119(38)	0.44892(37)	38.5(29)	46.9(33)	25.5(26)	-3.5(24)	-8.8(23)	1.5(22)
C(8)	0.05760(40)	0.13723(38)	0.47610(37)	38.3(29)	48.3(34)	27.9(27)	-2.1(25)	-4.1(23)	-2.6(23)
C(9)	0.00749(37)	0.13613(32)	0.41630(36)	35.1(27)	28.8(26)	28.3(25)	-2.0(20)	-2.8(21)	-1.0(20)
C(10)	-0.06589(37)	0.13351(34)	0.42180(34)	36.9(27)	31.0(27)	24.1(24)	-3.5(21)	2.9(21)	-0.1(19)
N(A1)	0.22919(36)	0.26792(41)	0.36927(43)	39.3(28)	37.8(27)	80.3(41)	-3.9(25)	-1.2(26)	-16.2(28)
C(A7)	0.24857(59)	0.33137(66)	0.36099(59)	44.3(42)	60.2(51)	81.2(55)	-7.7(42)	15.2(39)	10.4(43)
O(A1)	0.30982(47)	0.34738(49)	0.36541(69)	60.8(38)	95.5(48)	265.(11)	-22.3(35)	-4.6(51)	67.6(52)
C(A8)	0.19345(64)	0.38589(61)	0.34905(59)	72.3(53)	51.9(42)	64.7(49)	0.0(43)	31.4(41)	0.3(41)
C(A9)	0.12199(75)	0.36104(77)	0.3474(14)	59.7(59)	82.5(75)	393.(24)	23.6(51)	55.5(92)	81.(11)
C(A10)	0.20737(75)	0.42536(84)	0.28433(87)	106.4(78)	163.(10)	135.7(98)	47.3(70)	44.7(71)	92.1(86)
C(A11)	0.1992(15)	0.4303(10)	0.4142(12)	327.(24)	129.(11)	152.(14)	86.(14)	18.(14)	-55.(10)
N(B1)	-0.11332(51)	0.24709(41)	0.49828(41)	110.9(50)	32.5(27)	37.3(31)	4.5(32)	15.3(29)	-11.8(25)
C(B7)	-0.11312(80)	0.30487(81)	0.51568(60)	139.5(85)	81.7(71)	26.7(40)	12.9(67)	1.1(47)	5.7(48)
O(B1)	-0.11415(80)	0.32381(54)	0.58225(62)	308.(13)	85.3(50)	93.4(57)	-12.6(58)	-3.3(70)	1.8(45)
C(B8)	-0.10917(53)	0.36760(50)	0.46839(59)	53.2(40)	46.5(39)	61.8(46)	0.4(32)	-1.7(35)	4.5(37)
C(B9)	-0.17984(59)	0.39633(69)	0.45544(83)	49.8(47)	106.1(71)	178.(10)	2.6(47)	-8.9(55)	76.4(70)
C(B10)	-0.0798(10)	0.34676(74)	0.39818(90)	219.(14)	81.0(68)	120.2(91)	9.3(76)	82.6(93)	54.2(66)
C(B11)	-0.05914(79)	0.42026(73)	0.4928(10)	120.0(84)	82.6(68)	228.(15)	-31.1(63)	-108.8(92)	46.3(80)
C(A1)	0.24362(39)	0.14603(44)	0.35313(36)	34.3(29)	44.7(32)	25.5(26)	-0.7(26)	-2.7(21)	1.9(23)
C(A2)	0.28468(49)	0.08800(45)	0.35921(48)	48.5(38)	45.1(36)	58.8(42)	5.4(30)	-5.4(32)	13.0(30)
C(A3)	0.35398(54)	0.09234(61)	0.38525(59)	39.3(40)	76.0(56)	70.2(53)	15.4(36)	-8.1(36)	20.6(41)
C(A4)	0.38154(56)	0.15274(75)	0.40755(62)	45.1(45)	88.4(67)	70.4(53)	-3.3(46)	-28.1(38)	8.0(50)
C(A5)	0.34226(50)	0.21100(59)	0.40263(52)	36.0(36)	76.2(52)	63.1(46)	-10.8(35)	-14.6(32)	-6.5(40)
C(A6)	0.27242(44)	0.20947(50)	0.37532(43)	35.6(33)	51.2(38)	45.6(35)	-2.9(29)	-3.3(26)	-6.5(30)
C(B1)	-0.09457(36)	0.12697(43)	0.49727(38)	35.2(27)	40.5(31)	29.2(27)	0.2(25)	0.2(21)	4.7(26)
C(B2)	-0.09746(42)	0.06311(45)	0.53027(45)	47.8(35)	47.6(36)	39.7(36)	-0.8(27)	2.9(28)	6.2(28)
C(B3)	-0.12192(51)	0.05664(55)	0.59986(54)	58.0(43)	66.2(49)	40.0(41)	-7.8(35)	4.2(32)	18.6(35)
C(B4)	-0.14257(46)	0.11303(65)	0.63653(45)	48.2(36)	79.3(53)	29.1(33)	-4.1(40)	9.3(26)	15.6(37)
C(B5)	-0.14079(44)	0.17535(52)	0.60584(42)	50.5(36)	66.6(44)	24.1(30)	6.0(32)	8.6(26)	-1.0(29)
C(B6)	-0.11641(42)	0.18324(48)	0.53546(41)	46.5(33)	47.9(36)	27.0(30)	-0.1(28)	3.2(24)	6.4(27)

[a] Estimated standard deviations in the least significant figure(s) are given in parentheses in this and all subsequent tables. [b] The form of the anisotropic thermal ellipsoid is: $\exp[-(b11h^2 + b22k^2 + b33l^2 + 2b12hk + 2b13hl + 2b23kl)]$. The quantities given in the table are the thermal coefficients $\times 10^4$.

structure and II were nonroutine more detail than usual is supplied.

From a sharpened, origin-removed Patterson synthesis coordinates for the iron atom and the two crystallographically independent porphyrinato nitrogen atoms were deduced. Positions for remaining nonhydrogen atoms were obtained from Fourier syntheses interspersed with structure factor calculations and cycles of least-squares refinement. Initial refinements were on F and utilized only those 2268 reflections having $F_o^2 > 3\sigma(F_o^2)$. Disorder of the 2-MeIm ligand about the crystallographic twofold axis leads to near superposition of atomic positions. Consequently, in rigid group refinements of this moiety, its geometry was constrained to that shown in Figure 1, which also defines the atom labeling scheme for the remainder of the molecule. Initially the phenyl rings were constrained to D_{6h} symmetry (C-C = 1.395 Å). All atoms in rigid groups were allowed individual isotropic thermal parameters. Values for R and R_w of 0.156 and 0.190, respectively, were obtained after two cycles of least-squares refinement of a model comprising 30 atoms (each with an isotropic thermal parameter) and three rigid groups (two phenyl and one 2-MeIm). However, the ill-defined solvate species, ethanol, which was disordered about the twofold axis continued to refine unreasonably and hence in subsequent calculations its geometry was constrained in a rigid group (C-C = 1.541 Å, C-O = 1.465 Å, C-C-O = 109.5°).

Atoms not constrained in rigid groups were now assigned an anisotropic model for their thermal motion. Two cycles of least-squares refinement yielded values for R and R_w on F of 0.115 and 0.136, respectively. A search for hydrogen atoms was then conducted. The very high apparent thermal motion of the methyl carbon atoms of the pivalamide groups precluded an entirely unambiguous location of the methyl hydrogen atoms. Nonetheless, all hydrogen atoms, with the exceptions of those on the solvate species and the pivalamide nitrogen atoms, were included at their calculated idealized positions as a fixed

Table III. Rigid Group Parameters for Fe(TpivPP)(2-MeIm)·EtOH

ATOM	X	Y	Z	$B, Å^2$	ATOM	X	Y	Z	$B, Å^2$
IN(1)	0.01409(57)	0.01099(30)	0.23843(61)	4.94(26)	EO(1)	-0.0564(19)	-0.2272(15)	0.3001(15)	17.9(13)
IN(2)	0.00658(70)	-0.10260(30)	0.24701(71)	6.47(24)	EC(1)	-0.0305(14)	-0.28209(95)	0.2533(15)	7.97(87)
IC(1)	-0.01589(46)	-0.04256(34)	0.27040(48)	6.17(39)	EC(2)	-0.0036(18)	-0.2507(16)	0.1823(13)	8.27(96)
IC(2)	0.05492(60)	-0.08768(47)	0.19585(62)	6.49(38)	EO(2)	0	-0.4709(17)	1/4	22.3(11)
IC(3)	0.05733(47)	-0.01996(48)	0.19292(51)	6.69(43)	EC(3)	-0.0411(17)	-0.4101(17)	0.2280(35)	22.3(11)
IC(ME)	-0.07166(60)	-0.03393(65)	0.32926(61)	6.65(42)	EC(4)	0	-0.3445(17)	1/4	22.3(11)

RIGID GROUP PARAMETERS

GROUP	X_C	Y_C	Z_C	DELTA	EPSILON	ETA
IMD1	0.02072(42)	-0.03126(31)	0.23166(45)	0.1514(78)	-2.9887(76)	-0.8024(44)
ETOH-1	-0.0564(18)	-0.2272(15)	0.3001(15)	0.011(43)	2.932(24)	-1.155(25)
ETOH-2	0	-0.3445(17)	1/4	-1.5708	-2.681(84)	0

[a] X_C, Y_C, and Z_C are the fractional coordinates of the origin of the rigid group. [b] The rigid group orientation angles delta, epsilon, and eta(radians) have been defined previously: La Placa, S. J.; Ibers, J. A. *Acta Crystallogr.*, **1965,** *18,* 511-519.

contribution to F_c. A C-H separation of 0.95 Å and, for methyl hydrogen atoms, a C-C-H bond angle of 109.5° were assumed. The thermal parameter for a hydrogen atom was fixed at 1.0 $Å^2$ greater than the equivalent isotropic thermal parameter of its attached carbon atom.

When, after further cycles of least-squares refinement, now on F^2 and using all data including $F_o^2 < 0$, a region of electron density along and near the twofold axis persisted, a closer investigation of the solvate species was undertaken. As ill-resolved solvate species also plagued the structure analysis of II, parallel calculations were performed on both structures in the hope that the problem could be unraveled in a synergistic manner. As deduced from Fourier maps, the best model for I and also for II, judged both on chemical grounds and by subsequent successful least-squares refinement, involved the disorder of one ethanol molecule per asymmetric unit over two crystallographically independent sites. At one site (occupancy α) the ethanol oxygen atom was hydrogen bonded to the noncoordinating nitrogen atom of the imidazole ligand. The other site (occupancy $1 - \alpha$) was also close to the twofold axis but was considerably further from the imidazole ligand. There is additional disorder created by the twofold axis.

Group constraints on the phenyl rings were relaxed and this final model, described by 373 variable parameters, was refined to satisfactory convergence. The final values for R and R_w on F^2 are 0.140 and 0.204, respectively, and the standard error in an observation of unit weight is 1.62 e^2. For the portion of data having $F_o^2 > 3\sigma(F_o^2)$ the conventional values of R and R_w on F are 0.086 and 0.098. The final value for the ethanol occupancy parameter α is 0.68 (2), but because of correlation the final thermal parameters and the distribution of the ethanol molecule between the two solvate sites should not be taken too seriously. There was some dependence of the minimized function on $|F_o|$ and $\lambda^{-1} \sin \theta$, but this may be attributed to the inadequacies in this or any other model in coping with the very high thermal motion and/or unresolved disorder which afflicts many parts of the structure. The final difference Fourier synthesis was mostly flat and featureless, with the highest peaks being near the iron atom (height 1.01 (9) e $Å^{-3}$); the height of the next peak is 0.58 e $Å^{-3}$. In earlier syntheses peaks associated with the minor solvate site (final refined occupancy 32%) had been in the range 0.82-0.58 e $Å^{-3}$. Tables II and III contain final nonhydrogen atomic parameters. Hydrogen atom parameters are given in Table IV.[31] Table V lists the values of $10|F_o|$ vs. $10|F_c|$.[31] A negative entry indicates that $F_o^2 \leq 0$.

Solution and Refinement of Structure II. Starting from the coordinates for the *meso*-tetraphenylporphyrinato component of I, the structure of II was developed in a similar manner with only those 3205 reflections having $F_o^2 > 3\sigma(F_o^2)$ being utilized initially. As in I, the methyl carbon atoms of each pivalamide group were observed as three distinct, though diffuse, regions of electron density; disorder similar to that observed for the $Fe(O_2)$(TpivPP)(1-MeIm) structure[12] was not apparent. Unfortunately, the terminal oxygen atom for II occupied, unequally, two crystallographically independent sites, and hence suffered from disorder. In order to establish a meaningful overall occupancy for the dioxygen molecule and a meaningful apportionment of the terminal atom between its two sites the following refinement was conducted. Variable occupancies, β and γ, were assigned to the bonded oxygen atom and one terminal oxygen site, respectively; the occupancy of the other was constrained to be $\beta - \gamma$. Isotropic thermal parameters described the thermal motion of the dioxygen ligand; these for the two terminal oxygen positions were constrained to be equal. In other respects the refinement paralleled the isotropic refinement of I described above. Values for β and γ of 0.93 (3) and 0.54 (3) were obtained after two cycles of refinement. At this stage the values for R and R_w on F were 0.149 and 0.196.

The thermal parameters of nongroup atoms were now allowed to vary anisotropically. After three cycles of least-squares refinement, which lowered values for R and R_w on F to 0.107 and 0.138, a search for hydrogen atoms was made. All hydrogen atoms, with the exception of those on the solvate species, were included as a fixed contribution to F_c. After the solvate species was charac erized, as described above for I, refinements on all data, including $F_o^2 < 0$, were commenced. Because of correlation between occupancy and (anisotropic) thermal parameters for the dioxygen molecule which occurred in the previous three cycles and also because a better model for the solvate species was now being employed, more meaningful constraints were applied to the dioxygen moiety and the relative occupancy of the two terminal sites was reassessed. The occupancy parameter β was fixed at 1.0; otherwise the refinement was as previously described. A value for γ of 0.602 (17) was obtained. This value of γ was now held constant and thermal parameters for the dioxygen molecule were allowed to vary anisotropically. Group constraints on the phenyl rings were relaxed and this final model, specified by 396 variable parameters, was refined to satisfactory convergence with final values for R and R_w on F^2 of 0.119 and 0.214 and with a standard error in an observation of unit weight of 1.92 e^2. For the portion of data having $F_o^2 > 3\sigma(F_o^2)$ the values of R and R_w on F are 0.083 and 0.104. The final value for α, the occupancy of the hydrogen-bonded solvate species, is 0.45 (2), but interpretation of the final values for the thermal parameters and occupancies of the solvate species must again be made with caution. Furthermore, there was also a dependence of the value of the minimized function on $|F_o|$ and $\lambda^{-1} \sin \theta$. Except for a peak near the iron atom (height 0.95 (7) e $Å^{-3}$), the final difference Fourier map is flat and featureless with the second highest peak having a height of 0.46 e $Å^{-3}$. Tables VI and VII list the final nonhydrogen parameters for II. Hydrogen atom parameters are given in Table VIII.[31] Table IX lists the values of $10|F_o|$ vs. $10|F_c|$.[31] A negative entry indicates $F_o^2 \leq 0$.

Solid State Oxygen Equilibria. The simple manometric adsorption apparatus and techniques used to determine dioxygen adsorption isotherms for these solid samples are essentially the same as those previously described.[18,32] In studies using an ethanol-saturated atmosphere, the sample volume contained a subcompartment filled with

Table VI. Final Atomic Parameters for $Fe(O_2)$(TpivPP)(2-MeIm)·EtOH

ATOM	X	Y	Z	B11	B22	B33	B12	B13	B23
FE	0	0.134065(59)	1/4	29.24(35)	40.17(42)	30.13(38)	0	-1.60(27)	0
O(1)	0	0.23165(33)	1/4	65.1(33)	40.1(23)	70.7(34)	0	-5.3(26)	0
O(2A)	0.0163(16)	0.2707(10)	0.2021(14)	64.4(99)	53.4(67)	119.(13)	-6.1(70)	15.7(98)	48.2(79)
O(2B)	0.0470(16)	0.2711(16)	0.2718(28)	70.(15)	63.(12)	127.(23)	-42.(11)	-24.(17)	-17.(14)
N(1)	0.09638(19)	0.14003(19)	0.20775(19)	30.1(12)	30.8(13)	31.0(14)	-0.7(10)	-1.5(10)	0.3(11)
C(1)	0.11322(25)	0.14049(24)	0.13434(25)	33.2(16)	33.7(17)	31.8(17)	0.8(13)	1.5(13)	0.6(14)
C(2)	0.18946(27)	0.14580(28)	0.12696(29)	34.7(18)	46.7(22)	40.8(21)	-3.0(16)	5.5(15)	2.5(17)
C(3)	0.21757(26)	0.14806(28)	0.19490(31)	29.9(17)	45.0(21)	48.3(23)	-1.2(14)	-0.9(16)	-2.5(17)
C(4)	0.16013(25)	0.14405(24)	0.24538(26)	31.8(16)	30.4(16)	36.8(18)	0.2(13)	-1.1(13)	-1.7(14)
C(5)	0.16954(24)	0.14268(23)	0.32072(26)	33.1(16)	28.7(16)	35.6(17)	1.1(13)	-4.8(13)	0.0(14)
N(2)	0.04257(18)	0.13703(18)	0.35096(19)	31.5(13)	25.1(11)	32.2(13)	-0.34(98)	-1.4(10)	1.1(10)
C(6)	0.11437(24)	0.13940(23)	0.37032(25)	32.4(16)	25.1(14)	36.2(17)	-0.2(12)	-4.1(13)	-0.3(13)
C(7)	0.12297(27)	0.13786(27)	0.44787(26)	36.8(18)	45.6(20)	32.4(17)	-1.2(16)	-7.7(14)	1.6(16)
C(8)	0.05963(29)	0.13537(27)	0.47614(27)	41.5(20)	42.5(19)	33.4(18)	-4.8(16)	-2.5(15)	-0.5(16)
C(9)	0.00825(25)	0.13466(23)	0.41562(24)	35.0(16)	29.2(15)	29.4(15)	-0.1(13)	-0.1(13)	0.1(13)
C(10)	-0.06501(25)	0.13626(23)	0.42355(25)	36.6(17)	26.5(14)	33.2(16)	-1.2(13)	2.6(13)	0.1(13)
N(A1)	0.23246(24)	0.26735(27)	0.36901(32)	32.2(16)	42.3(19)	93.0(30)	-4.6(14)	-4.8(17)	-15.3(19)
C(A7)	0.25309(36)	0.33119(36)	0.35956(37)	41.1(24)	47.3(26)	69.8(32)	-7.2(20)	7.2(21)	2.5(22)
O(A1)	0.31435(29)	0.34582(30)	0.36293(47)	45.1(21)	74.6(27)	221.5(61)	-13.7(18)	6.1(28)	48.1(31)
C(A8)	0.19719(38)	0.38588(33)	0.35024(42)	55.8(29)	40.4(24)	67.5(32)	-2.8(20)	7.6(24)	-4.3(22)
C(A9)	0.12657(56)	0.36899(67)	0.3682(10)	62.9(43)	120.3(71)	348.(17)	42.9(45)	83.4(71)	121.2(88)
C(A10)	0.19769(89)	0.4125(11)	0.28046(82)	194.(11)	279.(14)	122.0(80)	180.(11)	81.7(78)	115.6(96)
C(A11)	0.21584(90)	0.44040(76)	0.4011(14)	145.(10)	104.1(72)	395.(24)	35.9(66)	-54.(12)	-123.(11)
N(B1)	-0.10949(32)	0.25089(28)	0.50227(26)	98.0(32)	34.8(17)	35.0(18)	4.6(19)	14.2(18)	-3.5(15)
C(B7)	-0.11182(44)	0.31229(45)	0.52300(40)	86.6(39)	61.5(34)	41.5(27)	0.9(28)	7.6(25)	1.7(26)
O(B1)	-0.12209(51)	0.32691(35)	0.59012(41)	226.5(68)	69.9(28)	81.5(33)	5.3(33)	11.6(37)	-3.9(25)
C(B8)	-0.10848(36)	0.37162(34)	0.47262(41)	50.4(25)	41.3(23)	65.9(31)	2.2(20)	2.7(22)	7.7(23)
C(B9)	-0.17929(45)	0.39718(61)	0.45563(66)	50.0(33)	135.1(63)	160.1(75)	-7.0(36)	-8.8(39)	90.5(57)
C(B10)	-0.07283(84)	0.35266(56)	0.40568(77)	218.(11)	72.5(49)	153.7(83)	28.8(55)	103.9(81)	59.3(53)
C(B11)	-0.06602(66)	0.42919(52)	0.50228(83)	136.3(70)	73.7(46)	221.(10)	-36.3(45)	-116.0(71)	44.4(55)
C(A1)	0.24348(26)	0.14530(28)	0.35138(27)	30.2(16)	42.8(20)	39.4(19)	1.7(15)	-3.9(14)	4.0(16)
C(A2)	0.28405(32)	0.08651(32)	0.35659(36)	42.2(23)	45.5(23)	68.1(30)	7.0(18)	-6.0(20)	7.2(21)
C(A3)	0.35400(37)	0.08928(44)	0.38146(43)	41.4(26)	66.2(33)	84.7(39)	11.3(24)	-10.3(25)	19.4(29)
C(A4)	0.38200(37)	0.15047(53)	0.40391(46)	38.3(25)	86.7(45)	85.9(41)	-1.7(28)	-22.5(25)	14.0(34)
C(A5)	0.34321(35)	0.20957(40)	0.40147(40)	38.4(23)	62.0(31)	84.2(38)	-3.2(22)	-19.9(23)	-4.6(26)
C(A6)	0.27412(28)	0.20732(32)	0.37437(32)	31.3(18)	47.4(23)	56.1(26)	-2.6(17)	-5.6(17)	-4.4(19)
C(B1)	-0.09339(26)	0.12941(28)	0.49990(26)	36.9(17)	38.8(18)	30.1(16)	-2.7(15)	1.9(13)	3.3(15)
C(B2)	-0.09692(29)	0.06521(29)	0.53231(31)	45.3(22)	41.8(21)	45.8(23)	-2.5(16)	0.4(18)	10.5(18)
C(B3)	-0.12158(33)	0.05929(36)	0.60339(36)	48.6(24)	54.5(27)	49.1(27)	-2.2(20)	2.9(20)	20.3(22)
C(B4)	-0.14268(32)	0.11487(41)	0.64022(33)	44.4(23)	68.0(32)	38.5(23)	1.9(21)	5.1(18)	13.5(22)
C(B5)	-0.13904(32)	0.17994(36)	0.60869(31)	55.2(25)	56.8(26)	35.8(22)	2.0(20)	7.9(18)	-1.2(19)
C(B6)	-0.11428(28)	0.18689(31)	0.53824(28)	44.9(21)	44.5(21)	31.8(19)	1.7(16)	5.0(15)	3.6(17)

ethanol. This contributed a constant and measurable background of ~60 Torr at 25 °C. The electric manometer, a Datametrics Inc. Barocell Model 1174-570, was calibrated against a new MKS Instruments Inc. Barotron, Model 310BHS-1000, over the full range of the instrument (0–1000 Torr), and found to agree to within 0.1% and to be reproducible to within 0.5% of the observed pressure for measurements made under ethanol. The errors in the determination of moles of O_2 adsorbed were generally less than 3%; in the absence of ethanol errors were less than 0.5%.

By extrapolation to infinite O_2 pressure the stoichiometry of O_2 binding was established to be 1 mol of dioxygen per mol of iron to within 1% in all cases. Complete reversibility was observed with each sample; data were collected at random over the range of O_2 pressures used. In the absence of ethanol, even after 50 cycles between O_2 and vacuum, no discernible change had occurred in the binding of dioxygen by the sample (to within experimental error, <0.5% of moles of O_2 adsorbed). For Fe(TpivPP)(2-MeIm)·EtOH under ethanol vapor, oxidation occurred more rapidly, although it was still less than 5% after 25 cycles. In all cases dioxygen binding studies have been made on at least two separately prepared samples using both adsorption and desorption techniques. The desolvated Fe(TpivPP)(2-MeIm) could be prepared in situ from Fe(TpivPP)(2-MeIm)·EtOH by simple evacuation without disassembly or recalibration. In this way the dramatic differences in their O_2 binding properties were confirmed.

In studies of Fe(TpivPP)(2-MeIm)·EtOH solvate analyses were performed before and after oxygenation studies; the EtOH:Fe ratios (0.9 (1):1) were determined by vapor phase chromatography of pyridine solutions. Elemental analyses, magnetic susceptibilities (under Ar and O_2), and visible spectra were in excellent agreement with the presumed compositions for I and II.[18]

Table VII. Rigid Group Parameters for $Fe(O_2)$(TpivPP)(2-MeIm)·EtOH

ATOM	X	Y	Z	B,Å^2	ATOM	X	Y	Z	B,Å^2
IN(1)	0.01083(43)	0.02659(21)	0.24130(46)	4.93(16)	EO(1)	-0.0527(13)	-0.2072(12)	0.3051(13)	4.11(79)
IN(2)	0.00346(52)	-0.08695(21)	0.24822(53)	6.08(14)	EC(1)	-0.0350(17)	-0.26363(93)	0.2558(14)	10.0(12)
IC(1)	-0.01920(32)	-0.02736(24)	0.27262(33)	6.08(25)	EC(2)	0.0155(22)	-0.2374(23)	0.1971(21)	11.1(12)
IC(2)	0.05199(45)	-0.07130(32)	0.19706(47)	6.59(25)	EO(2)	0	-0.4758(17)	1/4	29.9(11)
IC(3)	0.05431(35)	-0.00363(33)	0.19512(38)	6.50(25)	EC(3)	-0.0358(26)	-0.4151(17)	0.2194(32)	29.9(11)
IC(ME)	-0.07522(43)	-0.01962(47)	0.33188(44)	7.00(28)	EC(4)	0	-0.3496(17)	1/4	29.9(11)

RIGID GROUP PARAMETERS

GROUP	X$_C$	Y$_C$	Z$_C$	DELTA	EPSILON	ETA
IMID	0.01756(29)	-0.01550(21)	0.23387(31)	0.1538(61)	-2.9753(60)	-0.7964(36)
ETOH-1	-0.0527(13)	-0.2072(12)	0.3051(12)	-0.337(53)	3.077(30)	-0.960(27)
ETOH-2	0	-0.3496(16)	1/4	-1.5708	-2.464(88)	0

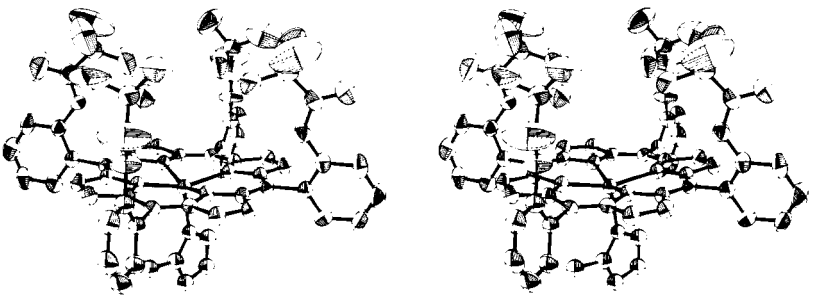

Figure 2. Stereodiagram of Fe(TpivPP)(2-MeIm). Ellipsoids are drawn at the 30% probability level. Hydrogen atoms are omitted for clarity.

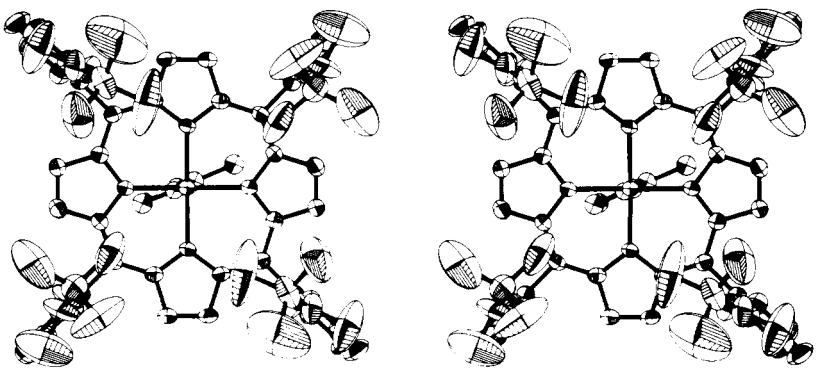

Figure 3. Stereodiagram of Fe(TpivPP)(2-MeIm) looking down the twofold axis. Ellipsoids are drawn at the 30% probability level. Hydrogen atoms are omitted for clarity.

Results and Discussion

General Description of the Structures. The deoxy complex, Fe(TpivPP)(2-MeIm)·EtOH (I), is illustrated in Figures 2 and 3. In order that small differences may be better appreciated, perspectives and orientation are identical for the corresponding diagrams, Figures 4 and 5, of the dioxygen complex $Fe(O_2)$(TpivPP)(2-MeIm)·EtOH (II). Similarly, Figures 6 and 7 show the arrangements of I and II in the unit cells.

The twofold symmetry, which is imposed on molecular species, leads to disorder about the crystallographic twofold axis of the 2-methylimidazole ligand, the ethanol of solvation, and, for II, the angularly bound dioxygen ligand. The ethanol solvate species suffers from additional disorder: in one of its two crystallographically independent sites it is weakly hydrogen bonded to the 2-MeIm ligand. The N-H···O separations are 2.88 (3) Å for I and 2.78 (2) Å for II. Near superposition of atomic positions for the 2-MeIm and the ethanol moieties necessitated the application of rigid group constraints. For the 2-MeIm ligand an idealized geometry was used (see Figure 1). Small systematic errors in parameters associated with this group may, therefore, exist, but *differences* in parameters between I and II are meaningful. Because Fourier maps of the solvate species were ill resolved and interpretation is not unambiguous, intermolecular contacts involving these atoms may well be in considerably greater error than that indicated by least-squares refinement. The dioxygen ligand in II shares a generally similar angular geometry and disorder with its 1-MeIm analogue. The occupancy ratio for the two crystallographically independent terminal oxygen atom sites is 0.60 (2):0.40. As previously observed[11,12] the Fe-O-O planes approximately bisect the N_p-Fe-N_p right angles. The O-O separations and Fe-O-O bond angles are uncorrected for the effects of thermal motion and/or a small off-axis displacement of the coordinated oxygen atom which could be inferred from

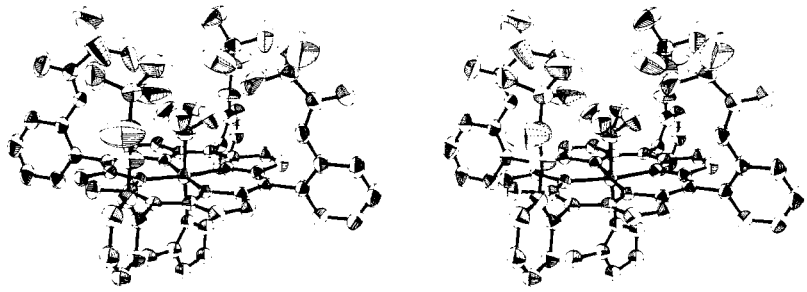

Figure 4. Stereodiagram of $Fe(O_2)$(TpivPP)(2-MeIm). Ellipsoids are drawn at the 30% probability level. Disorder of the terminal oxygen atom but not of the 2-MeIm is shown. Hydrogen atoms are omitted for clarity.

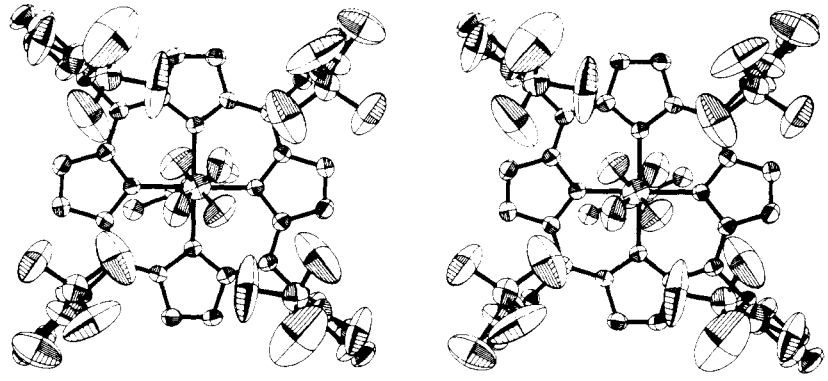

Figure 5. Stereodiagram of $Fe(O_2)$(TpivPP)(2-MeIm) looking down the twofold axis. Ellipsoids are drawn at the 30% probability level. Disorder of the terminal oxygen atom but not of the 2-MeIm is shown. Hydrogen atoms are omitted for clarity.

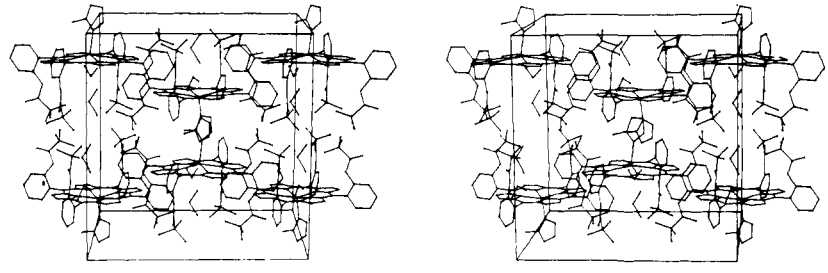

Figure 6. Stereodiagram of the unit cell for Fe(TpivPP)(2-MeIm)·EtOH. The two crystallographically independent ethanol moieties are shown. Hydrogen atoms are omitted for clarity. The view is approximately down the *c* axis; the *b* axis is vertical.

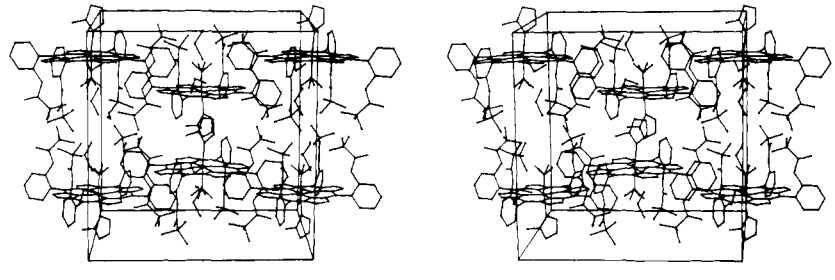

Figure 7. Stereodiagram of the unit cell for $Fe(O_2)$(TpivPP)(2-MeIm)·EtOH. The two crystallographically independent ethanol moieties are shown; disorder of the terminal oxygen atom but not of the 2-MeIm is shown. Hydrogen atoms are omitted for clarity. The view is approximately down the *c* axis; the *b* axis is vertical.

the flattened shape of its thermal ellipsoid (root mean square components of displacement are 0.277 (8), 0.329 (9), and 0.362 (8) Å). Nonetheless, we have defined more precisely than before a lower bound for the O–O separation (1.21 (2) Å) and an upper bound for the Fe–O–O angle (129 (1)°). Comprehensive compilations of bond distances and angles are available in Tables X and XI. The isolation of a nondisordered, iron–dioxygen complex obviously remains a high priority.

In common with all other "picket-fence" porphyrin structures,[12,33,34] atoms of the pivalamide "pickets" are afflicted with very high thermal motion and/or irresolvable disorder. However, the immediate coordination sphere and the porphyrinato skeleton are reasonably precisely defined, although for the dioxygen complex the scatter of formally chemically equivalent parameters about their mean is a little larger than that expected from the estimated standard deviation of an individual parameter (see Figure 8 and Tables X and XI). Inspection of Figures 2–7 shows that oxygenation of I induces large changes only in the immediate coordination sphere; changes in crystal packing and the porphyrin periphery are

Table X. Bond Distances (Å)[a] for I and II

atoms	distance		atoms	distance	
Fe-N(1)	2.068(5)	1.997(4)	Fe-N(2)	2.075(5)	1.995(4)
Fe-IN(1)	2.095(6)	2.107(4)	Fe-O(1)		1.898(7)
O(1)-O(2A)		1.205(16)	O(1)-O(2B)		1.232(22)
N(1)-C(1)	1.384(8)	1.387(6)	N(1)-C(4)	1.373(8)	1.373(6)
N(2)-C(6)	1.361(8)	1.392(6)	N(2)-C(9)	1.378(8)	1.363(6)
C(1)-C(2)	1.431(9)	1.452(7)	C(3)-C(4)	1.432(9)	1.443(7)
C(6)-C(7)	1.441(9)	1.424(6)	C(8)-C(9)	1.434(9)	1.453(6)
C(2)-C(3)	1.350(9)	1.339(7)	C(7)-C(8)	1.336(9)	1.315(7)
C(4)-C(5)	1.406(9)	1.385(6)	C(5)-C(6)	1.403(9)	1.399(6)
C(1)-C(10)	1.393(9)	1.381(6)	C(9)-C(10)	1.392(9)	1.394(6)
C(5)-C(A1)	1.503(9)	1.491(6)	C(10)-C(B1)	1.511(9)	1.514(6)
C(A1)-C(A2)	1.371(10)	1.378(7)	C(B1)-C(B2)	1.383(10)	1.385(7)
C(A2)-C(A3)	1.384(11)	1.386(8)	C(B2)-C(B3)	1.380(11)	1.396(8)
C(A3)-C(A4)	1.344(13)	1.361(10)	C(B3)-C(B4)	1.350(12)	1.340(8)
C(A4)-C(A5)	1.355(13)	1.363(10)	C(B4)-C(B5)	1.337(12)	1.393(9)
C(A5)-C(A6)	1.399(10)	1.383(7)	C(B5)-C(B6)	1.396(10)	1.388(7)
C(A6)-C(A1)	1.404(10)	1.398(7)	C(B6)-C(B1)	1.369(10)	1.382(7)
C(A6)-N(A1)	1.401(10)	1.410(7)	C(B6)-N(B1)	1.419(10)	1.412(7)
N(A1)-C(A7)	1.296(11)	1.314(7)	N(B1)-C(B7)	1.167(14)	1.254(8)
C(A7)-O(A1)	1.198(11)	1.190(7)	C(B7)-O(B1)	1.282(12)	1.279(8)
C(A7)-C(A8)	1.497(13)	1.505(9)	C(B7)-C(B8)	1.501(14)	1.479(9)
C(A8)-C(A9)	1.432(16)	1.419(11)	C(B8)-C(B9)	1.460(13)	1.452(10)
C(A8)-C(A10)	1.448(14)	1.377(12)	C(B8)-C(B10)	1.478(16)	1.459(13)
C(A8)-C(A11)	1.480(19)	1.448(15)	C(B8)-C(B11)	1.456(14)	1.472(11)
IN(2)-EO(1)	2.88(3)	2.78(2)			

[a] First entry is for Fe(TpivPP)(2-MeIm)·EtOH; second entry for $Fe(O_2)$(TpivPP)(2-MeIm)· EtOH.

generally small. Intra- and intermolecular structural changes upon oxygenation will be discussed after a closer examination of the stereochemistries of I and II.

The Deoxy Complex. Figure 9 summarizes some of the metrical details of the coordination spheres of I and II and two closely related compounds, Fe(TPP)(2-MeIm) and $Fe(O_2)$-(TpivPP)(1-MeIm). Differences between the Fe-N_p, Ct···N_p, or Fe···Ct separations for I and Fe(TPP)(2-MeIm) are of marginal significance and these first two distances are typical of other five-coordinate, high-spin metalloporphyrins, such as Mn(TPP)(1-MeIm).[35] However, the Fe-N_{Im} separation and the doming parameter—the difference between the Ct···Fe separation and the displacement of the iron atom from the least-squares plane of the 24-atom porphyrinato skeleton—are very different for I and Fe(TPP)(2-MeIm). The doming parameter, which is rarely larger than 0.05 Å,[34] and which for I is 0.026 Å, is 0.15 Å for Fe(TPP)(2-MeIm).[34] By way of comparison, the Ct···Mn separation for Mn(TPP)(1-MeIm) is 0.512 Å, yet the doming parameter[35] is only 0.045 Å. Construction of a space-filling model of the "picket-fence" porphyrin indicates that intramolecular steric interaction among the "pickets" should not prevent doming for "picket-fence" porphyrin complexes. Since TPP and TpivPP are very similar electronically the longer (by 0.066 Å) separation observed for Fe(TPP)(2-MeIm) could be attributed to the more nearly eclipsing conformation which the imidazole plane adopts with respect to the Fe-N_p bonds (see Figure 9).

The Oxy Complex. The Fe-N_p bond lengths and the Ct···N_p radius are typical of other low-spin iron(II) systems (see Table XII). However, the bulky 2-methyl substituent on the 2-MeIm ligand results in lengthened axial bonds relative to the sterically less demanding 1-MeIm ligand. The sum of the Fe-O and Fe-N_{Im} separations is 4.005 Å for II but only 3.813 Å for $Fe(O_2)$(TpivPP)(1-MeIm). Of this 0.192-Å difference, most (0.150 Å) arises from a *lengthening of the Fe-O bond* to a value similar to that observed for Schiff-base cobalt-dioxygen compounds. This lengthened Fe-O separation and also the greater sum may be correlated with the decreased dioxygen affinities in solution which have been observed for systems with hindered imidazoles.[4,18-20] Note also that atoms O, Fe, and

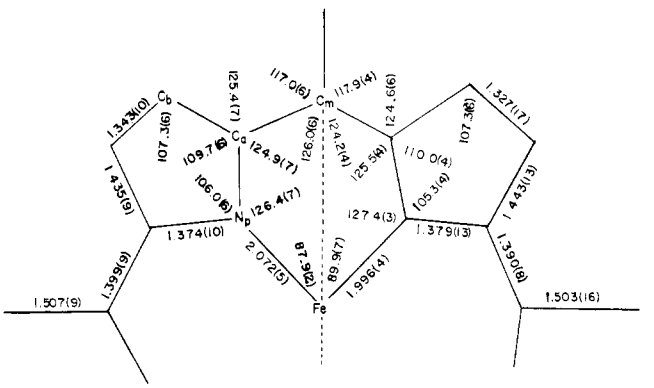

Figure 8. Averaged bond parameters for the porphyrinato skeleton for I and II. Parameters for I are to the left of the dotted line; those for II are to the right. The general labeling scheme for porphyrinato species is also shown.

N_{Im} are collinear for $Fe(O_2)$(TpivPP)(1-MeIm); for II the angle is 172.9 (2)°.

For II, the compromise between maximum bonding and minimum destabilizing nonbonding contacts results in the iron atom remaining 0.086 Å out of the plane of the porphyrinato nitrogen atoms toward the 2-MeIm ligand. This is in marked contrast to that observed for $Fe(O_2)$(TpivPP)(1-MeIm) where the displacement is 0.03 Å out of the plane toward the dioxygen ligand and for other related compounds whose stereochemistries are summarized in Table XII. The porphyrinato-dioxygen contacts for II and $Fe(O_2)$(TpivPP)(1-MeIm) are not significantly different, dispelling the slight reservations expressed about the accuracy of the Fe-O separation for $Fe(O_2)$-(TpivPP)(1-MeIm).[12]

Structural Changes Occurring upon Oxygenation. A. Intramolecular. The expected contractions in the average Fe-N_p separation (0.076 Å) and in the Ct···N_p radius (0.039 Å), attributable to the transition from the five-coordinate, high-spin, deoxy form to the six-coordinate, low-spin, oxy form are observed, as well as a general contraction of the porphyrinato skeleton. The average change in the separation of dyadically

Table XI. Bond Angles (deg)[a] for I and II

atoms	angle		atoms	angle	
N(1)-Fe-N(1)′	158.0(3)	173.2(2)	N(2)-Fe-N(2)	157.5(3)	176.7(2)
N(1)-Fe-N(2)	87.9(2)	90.4(1)	O(1)-Fe-IN(1)	170.4(3)[b]	172.9(2)
N(1)-Fe-N(2)′	87.8(2)	89.4(1)			
N(1)-Fe-IN(1)	91.9(3)	86.4(2)	N(2)-Fe-IN(2)	103.7(3)	93.5(2)
O(1)-Fe-N(1)		86.7(1)	O(1)-Fe-N(2)		88.3(1)
Fe-O(1)-O(2A)		129.0(12)	Fe-O(1)-O(2B)		128.5(18)
Fe-IN(1)-IC(1)	132.1(8)	135.0(6)	Fe-IN(1)-IC(3)	126.3(7)	123.3(5)
Fe-N(1)-C(1)	126.3(4)	127.4(3)	Fe-N(2)-C(6)	126.8(4)	127.0(3)
Fe-N(1)-C(4)	127.0(4)	127.2(3)	Fe-N(2)-C(9)	125.5(4)	127.8(3)
C(1)-N(1)-C(4)	105.8(6)	105.4(4)	C(6)-N(2)-C(9)	106.2(5)	105.1(4)
N(1)-C(1)-C(2)	109.3(6)	110.0(4)	N(2)-C(6)-C(7)	110.0(6)	109.8(4)
N(1)-C(4)-C(3)	110.3(6)	110.2(4)	N(2)-C(9)-C(8)	109.2(6)	109.8(4)
N(1)-C(1)-C(10)′	124.5(6)	125.4(4)	N(2)-C(6)-C(5)	125.1(6)	124.9(4)
C(2)-C(1)-C(10)′	126.2(7)	124.6(4)	C(7)-C(6)-C(5)	124.9(7)	125.4(4)
C(3)-C(4)-C(5)	124.8(7)	123.9(5)	C(8)-C(9)-C(10)	125.6(7)	124.4(4)
N(1)-C(4)-C(5)	124.8(6)	125.9(5)	N(2)-C(9)-C(10)	125.2(6)	125.7(4)
C(1)-C(2)-C(3)	107.8(6)	106.6(4)	C(6)-C(7)-C(8)	106.9(6)	108.1(4)
C(4)-C(3)-C(2)	106.7(6)	107.8(4)	C(9)-C(8)-C(7)	107.7(6)	107.2(4)
C(4)-C(5)-C(6)	125.8(6)	124.5(4)	C(9)-C(10)-C(1)′	126.2(6)	123.9(4)
C(4)-C(5)-C(A1)	116.6(6)	118.0(4)	C(9)-C(10)-C(B1)	116.8(6)	117.9(4)
C(6)-C(5)-C(A1)	117.6(6)	117.5(4)	C(1)′-C(10)-C(B1)	117.0(6)	118.1(4)
C(5)-C(A1)-C(A2)	121.2(8)	120.7(5)	C(10)-C(B1)-C(B2)	120.0(7)	119.7(5)
C(5)-C(A1)-C(A6)	119.8(7)	121.2(5)	C(10)-C(B1)-C(B6)	121.7(7)	120.6(5)
C(A2)-C(A1)-C(A6)	119.0(8)	118.1(5)	C(B2)-C(B1)-C(B6)	118.3(7)	119.7(5)
C(A1)-C(A2)-C(A3)	120.3(9)	120.9(6)	C(B1)-C(B2)-C(B3)	120.6(8)	119.6(6)
C(A2)-C(A3)-C(A4)	120.9(10)	119.5(7)	C(B2)-C(B3) -C(B4)	120.0(9)	120.8(6)
C(A3)-C(A4)-C(A5)	120.1(10)	121.6(6)	C(B3)-C(B4)-C(B5)	120.8(8)	120.4(6)
C(A4)-C(A5)-C(A6)	121.0(10)	119.0(7)	C(B4)-C(B5)-C(B6)	120.3(9)	119.6(6)
C(A5)-C(A6)-C(A1)	118.5(9)	120.9(6)	C(B5)-C(B6)-C(B1)	120.1(8)	119.9(5)
C(A5)-C(A6)-N(A1)	123.6(9)	121.1(6)	C(B5)-C(B6)-N(B1)	124.3(9)	123.0(6)
C(A1)-C(A6)-N(A1)	117.9(7)	117.9(5)	C(B1)-C(B6)-N(B1)	115.6(7)	117.0(5)
C(A6)-N(A1)-C(A7)	127.9(9)	128.7(5)	C(B6)-N(B1)-C(B7)	135.0(10)	134.1(6)
N(A1)-C(A7)-O(A1)	120.9(12)	120.6(7)	N(B1)-C(B7)-O(B1)	122.6(13)	120.6(7)
N(A1)-C(A7)-C(A8)	119.5(10)	118.3(6)	N(B1)-C(B7)-C(B8)	128.4(11)	123.5(7)
C(A8)-C(A7)-O(A1)	119.5(12)	120.9(7)	C(B8)-C(B7)-O(B1)	109.0(13)	115.7(8)
C(A7)-C(A8)-C(A9)	114.5(11)	118.0(7)	C(B7)-C(B8)-C(B9)	110.3(10)	110.3(7)
C(A7)-C(A8)-C(A10)	110.8(10)	110.5(7)	C(B7)-C(B8)-C(B10)	108.2(10)	110.7(7)
C(A7)-C(A8)-C(A11)	104.9(13)	106.7(9)	C(B7)-C(B8)-C(B11)	115.6(11)	113.3(8)
C(A9)-C(A8)-C(A10)	110.6(15)	109.2(12)	C(B9)-C(B8)-C(B10)	108.9(12)	110.4(10)
C(A9)-C(A8)-C(A11)	105.3(14)	103.6(12)	C(B9)-C(B8)-C(B11)	111.4(11)	109.9(8)
C(A10)-C(A8)-C(A11)	110.4(15)	108.2(13)	C(B10)-C(B8)-C(B11)	102.0(12)	104.1(10)
IN(2)-HIN(2)-EO(1)	166.8	166.0			

[a] First entry is for Fe(TpivPP)(2-MeIm)·EtOH; second entry for $Fe(O_2)$(TpivPP)(2-MeIm)·EtOH. [b] Angle quoted is that which the vector Fe-IN(1) makes with the twofold axis.

related porphyrinato atoms for I and II is 0.048 Å with extremes of 0.002 (atom C(10)) and 0.082 Å (atom N(2)). Atoms in phenyl group A move in while those in B move out slightly upon oxygenation (see Table XIII).[31]

While the orientation of the imidazole plane with respect to Fe-N_p vectors remains essentially constant upon oxygenation (Figure 9), its movement toward the porphyrinato plane "pushes" against the porphyrinato nitrogen atom, N(1); for I the four porphyrinato nitrogen atoms lie within 0.005 (5) Å of the least-squares plane but for II this increases to 0.030 (4) Å. The porphyrinato skeleton is rather buckled—the mean displacements from the least-squares plane of the 24-atom skeleton are 0.056 Å for I and a slightly greater 0.065 Å for II. The displacements are illustrated in Figure 10. The relative orientation of the pyrrole rings follows no systematic pattern and probably reflects the nonsymmetrical orientation of the imidazole ligand which neither bisects an N_p-Fe-N_p right angle nor eclipses an Fe-N_p vector (see Figure 9). Selected least-squares planes and the dihedral angles between them are presented in Tables XIV and XV.[31]

Upon oxygenation of the complex, the iron atom moves 0.316 Å toward but not into the plane of the porphyrinato nitrogen atoms, while preserving the Fe-N_{Im} separation. Nonbonding porphyrinato–imidazole contacts show decreases of up to 0.27 Å (Table XVI),[31] indicative of the strong bonding in low-spin, six-coordinate iron–porphyrinato complexes. The 2-MeIm ligand adjusts for this motion by increased tipping: the angles Fe-IN(1)-IC(1) and Fe-IN(1)-IC(3) increase their asymmetry upon oxygenation (see Table XI) while the angle of tilt between the Fe-N_p vector and the normal to the porphyrinato plane decreases from 9.6 to 7.1° (see also next section).

B. Intermolecular. Since crystallinity is maintained upon oxygenation large changes in intermolecular contacts are not expected nor are they observed. Changes in unit-cell dimensions are small and the small shrinkage in the *c* axis of 0.8% may be correlated with the general shrinkage of the porphyrinato skeleton. The iron atom and atoms belonging to the 2-MeIm and solvate moieties move substantially in a direction parallel to the *b* axis upon oxygenation. In addition, it is clear from Fourier maps, as well as from the final refined parameters, that the ill-resolved ethanol solvate species hydrogen bonded to the 2-MeIm ligand changes its orientation. But the remaining atoms show an average change in position of only 0.11 Å with a maximum of 0.44 Å for one of the pivalamide methyl carbon atoms, C(A11).[36]

Table XVII summarizes intermolecular contacts for I and II and also indicates the changes in contacts which occur when

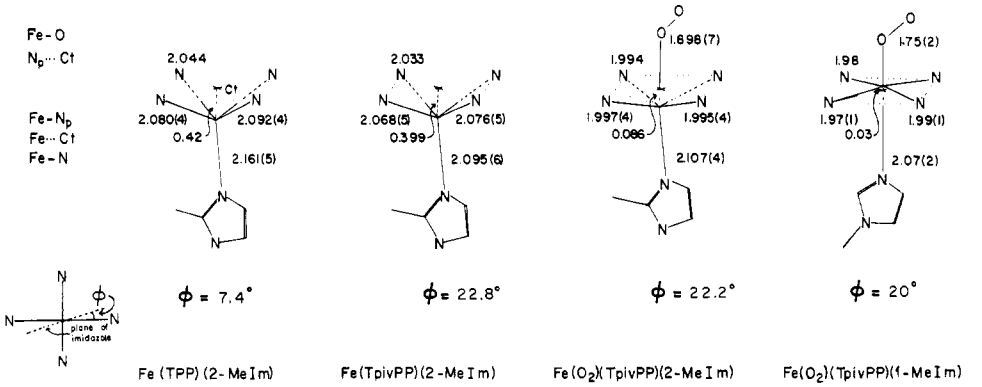

Figure 9. Structural changes upon oxygenation of an iron(II)(porphyrinato)(base) complex.

Table XII. Bond Parameters (Å) for Some Six-Coordinate, Low-Spin, Iron(II) Porphyrinato Compounds

compd	Fe-N_p	Fe-L	Fe-N_{Im}	Fe···Ct[a]
$Fe(O_2)$(TpivPP)-(1-MeIm)[b]	1.98(1)	1.75(2)	2.07(2)	+0.03
$Fe(O_2)$(TpivPP)-(2-MeIm)[c]	1.996(4)	1.898(7)	2.107(4)	−0.086
Fe(CO)(TPP)(py)[d]	2.02(3)	1.77(2)	2.10(1)	0.02
Fe(NO)(TPP)-(1-MeIm)[e]	2.008(9)	1.743(4)	2.180(4)	0.07
$Fe(TPP)(1\text{-MeIm})_2$[f]	1.997(4)		2.016(5)	0

[a] A negative value denotes a displacement toward the imidazole ligand. [b] Reference 12. [c] This work. [d] Reference 13. [e] Reference 14. [f] Hoard, J. L., personal communication.

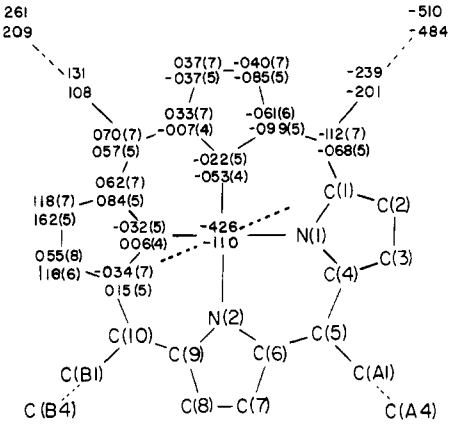

Figure 10. Displacements of atoms (Å $\times 10^3$) from the least squares plane of the 24-atom porphyrinato core. The displacements for I are quoted above those for II; the atom labeling system is indicated. Only those displacements with estimated standard deviations in parentheses were used to define the least-squares plane.

an oxygenated molecule is surrounded by deoxygenated molecules. Table XVIII[31] gives selected intermolecular contacts involving hydrogen atoms. For both I and II there are few contacts less than 3.5 Å. However, several of the shortest contacts involve atoms with very high apparent thermal motion and, hence, such separations cannot be regarded as realistic. This, together with the ill-resolved solvate species, cripples any attempt to perform meaningful, unbiased packing energy calculations. No dramatically close contacts arise when a molecule of II is surrounded by molecules of I, or vice versa. In other words, no single contact or group of contacts can be said clearly to influence the binding of dioxygen to I, Fe(TpivPP)(2-MeIm)·EtOH. Of the atoms with relatively modest thermal motion only contacts between phenyl-B and the 2-MeIm ligand show some rearrangement. The 2-MeIm ligand in I is tilted such that the O(A1)-IC(Me) contact is relieved (see also Figures 4 and 5). Upon oxygenation the 2-MeIm ligand moves away from this oxygen atom and the angle of tilt decreases from 9.6 to 7.1°. Moreover, the contraction of the porphyrinato core pulls in phenyl A and further reduces this contact.

Solid State Dioxygen Binding. The presence or absence of ethanol in the solid state dramatically affects dioxygen binding. The reversible binding of dixoygen to powdered samples of Fe(TpivPP)(1-MeIm), Fe(TpivPP)(1,2-Me_2Im), Fe(TpivPP)(2-MeIm), and Fe(TpivPP)(2-MeIm)·EtOH is shown in Figure 11 and collated in Table XIX. The binding of dioxygen under EtOH vapor to I, Fe(TpivPP)(2-MeIm)·EtOH, shows simple, noncooperative behavior over the range of 10–60% oxygenation with $P_{1/2}$ = 620 (30) Torr. This was surprising since Fe(TpivPP)(2-MeIm) without ethanol had already been found to bind dioxygen in a cooperative manner[18] (see Figure 11). This is not an experimental artifact, having been confirmed on several separately prepared samples, using both adsorption and desorption measurements. In addition, after being oxygenated under ethanol, a sample of Fe(TpivPP)(2-MeIm)·EtOH can be converted to Fe(TpivPP)(2-MeIm) by evacuation, and the O_2 binding of the desolvated solid regains its high affinity and cooperativity (with all measurements taken in the same apparatus without any disassembly or recalibration).

Having been able to gather X-ray diffraction data on both Fe(TpivPP)(2-MeIm)·EtOH and $Fe(O_2)$(TpivPP)(2-MeIm)·EtOH, we had hoped that the structures of these complexes and, especially, an analysis of the intermolecular contacts might have revealed the origin of the cooperativity observed in solid-state oxygenation. Unfortunately, since the solvated solids do not bind dioxygen cooperatively, we can only use these structures in a general way to speculate on the mechanism of cooperativity in this system. For I the motion of the 2-MeIm ligand toward the porphyrinato skeleton upon oxygenation is 0.30 Å and there is also a small contraction in the porphyrinato skeleton. Presumably, as molecules oxygenate, the change in molecular dimensions induces strain in the crystallite. Eventually this strain must be sufficient to induce a conformational change in the solid, which enhances the dioxygen affinity of the remaining deoxy sites. Why such a process occurs in some solids and not in others remains unknown. Indeed there is no a priori reason why cooperative and noncooperative rather than anticooperative behavior should be observed in the present system. Spin-crossover systems show similar cooperative behavior in the solid state as the ground spin states change with temperature. The nature of these spin transitions depends variously on crystal size, counterion and solvate choice, and defect content. Of particular interest here, the high-spin to low-spin transition of several Fe(II) complexes is dramatically influenced by the presence of solvate molecules. For example, bis(thiocyanato)bis(4,7-dimethyl-1,10-phen-

Table XVII. Intermolecular Contacts, Less Than 4.0 Å, for I (Deoxy) and II (Oxy) and for II Surrounded by Molecules of I

atoms	sym op[a]	deoxy[b] in deoxy	deoxy surrounded[c] by oxy in oxy cell	oxy in[d] oxy	$Fe(O_2)$(TpivPP)-(1-MeIm)[e]
C(2)-O(B1)	55405, 45505	3.86	3.67, 3.86	3.67	3.43
C(3)-O(B1)	55405, 45505	3.88	3.65, 3.87	3.65	3.48
C(6)—C(B3)	55606, 55606	3.88	3.93, 3.85	3.90	
C(7)-O(A1)	55607, 55607	3.63	3.62, 3.62	3.64	3.50
C(7)-C(B3)	55606, 55606	3.95	—, 3.88	3.95	
C(7)-C(B2)	55606, 55606		—, 3.96	4.00	
C(8)-O(A1)	55607, 55607	3.81	3.78, 3.77	3.75	3.53
C(8)-C(B2)	55606, 55606	3.97	—, 3.93	3.97	
C(A7)—E(O1)	4, 44504	—	3.98, 3.95	3.89	
O(A1)-IC(2)	8, 54508	3.08	3.28, 3.01	3.21	2.90
O(A1)-EO(1)	4, 44504	3.17	3.04, 3.07	2.93	
O(A1)-IC(ME)	4, 44504	3.29	3.44, 3.25	3.40	
O(A1)-IC(3)	8, 54508	3.77	—, 3.72	4.00	
O(A1)-EC(2)	8, —		3.88, —	3.78	
C(A10)-C(B4)	55405, —		3.99, —		
C(A11)-C(A3)	55607, —	3.88	3.91, —		
C(A11)-C(A4)	55607, —	4.00	—, —		
N(B1)-EC(2)	3, 55403	3.93	—, 3.81		
O(B1)-EC(2)	3, 55403	3.09	3.60, 3.14	3.65	
O(B1)-EC(3)	3, 55403	3.43	3.38, 3.33	3.31	3.24-3.64 solvate
O(B1)-EC(1)	3, 55403	3.58	3.67, 3.52	3.62	
O(B1)-EC(4)	3, 55403	3.74	3.74, 3.69	3.70	
C(B7)-EC(2)	3, 55403	3.81	—, 3.71		
C(B9)-C(B4)	45607, 45607	3.72	3.75, 3.73	3.76	
C(B9)-C(B5)	45607, 45607	3.80	3.88, 3.82	3.90	
C(B9)-C(B3)	45607, 45607	3.96	3.97, 3.96	3.97	
C(B11)-C(B11)	56606, —	3.82	3.76, —	3.72	
C(A3)-EC(3)	4, 44504	3.55	3.72, 3.47	3.66	
C(A3)-EC(4)	4, 44504	3.96	3.92, 3.92	3.89	3.54-3.75 solvate
C(A3)-EO(2)	4, 44504	3.96	3.98, 3.88	3.91	
C(A3)-EC(3)	8, —		3.97, —	3.94	
C(A4)-EO(1)	4, 44504	3.29	3.55, 3.28	3.54	
C(A4)-EC(2)	8, 54508	3.43	3.49, 3.41	3.48	
C(A4)-EC(1)	4, 44504	3.56	3.61, 3.50	3.58	
C(A4)-EC(4)	4, 44504	3.71	3.69, 3.63	3.63	
C(A4)-EC(3)	4, 44504	3.85	—, 3.75	3.96	3.42-3.71 solvate
C(A4)-EC(3)	8, —		3.99, —	3.93	
C(A5)-EO(1)	4, 44504	2.98	3.13, 2.95	3.12	
C(A5)-EC(2)	8, 54508	3.54	3.43, 3.51	3.42	
C(A5)-EC(1)	4, 44504	3.70	3.62, 3.66	3.60	
C(A6)-EO(1)	4, 44504	3.76	3.92, 3.73	3.91	
C(B3)-IC(1)	55606, 55606	3.50	3.54, 3.44	3.50	3.55 imid
C(B3)-IN(2)	55606, 55606	3.63	3.57, 3.55	3.51	
C(B3)-IC(1)	3, 55403	3.69	3.71, 3.62	3.66	
C(B3)-IN(2)	3, 55403	3.70	3.60, 3.62	3.54	
C(B3)-IC(2)	3, 55403	3.79	3.70, 3.74	3.66	
C(B3)-IN(1)	55606, 55606	3.80	3.89, 3.75	3.86	
C(B3)-IN(1)	3, 55403	3.81	3.91, 3.77	3.88	
C(B3)-IC(3)	3, 55403	3.82	3.85, 3.79	3.84	
C(B3)-IC(ME)	55606, 55606	3.87	3.96, 3.85	3.94	
C(B3)-IC(2)	55606, 55606	3.99	3.92, 3.89	3.85	
C(B3)-IC(3)	—, 55606		—, 3.96		
C(B4)-IN(2)	55606, 55606	3.31	3.36, 3.26	3.33	3.46 imid
C(B4)-IN(2)	3, 55403	3.44	3.43, 3.39	3.39	
C(B4)-IC(2)	55606, 55606	3.50	3.55, 3.43	3.50	
C(B4)-IC(1)	3, 55603	3.66	3.75, 3.62	3.73	
C(B4)-IC(1)	55606, 55606	3.67	3.82, 3.65	3.81	
C(B4)-EC(2)	3, 55403	3.83	3.98, 3.79	3.94	
C(B4)-IC(2)	3, 55403	3.89	3.89, 3.88	3.88	
C(B4)-IC(3)	—, 55606	3.93	—, 3.88		
C(B4)-IC(ME)	—, 55403		—, 4.00		
C(B4)-EO(1)	3, 55403		3.93, 3.97	3.87	
C(B5)-EC(2)	3, 55403	3.26	3.56, 3.17	3.48	
C(B5)-IN(2)	55606, 55606	3.93	—, 3.89		
C(B5)-EC(1)	3, 55403	3.97	3.77, 3.85	3.67	
C(B5)-EO(1)	3, 55403		—, 3.91	3.94	
C(B5)-EO(1)	55606, —		—, —	3.94	
C(B6)-EC(2)	3, 55403	3.64	3.96, 3.55	3.88	
IN(2)-EO(1)	1	2.88		2.78	
IN(2)-EC(2)	1	3.12		3.08	
IN(2)-EC(1)	1	3.56		3.52	
IC(1)-EO(1)	1	3.71		3.61	

Table XVII (*Continued*)

atoms	sym op[a]	deoxy[b] in deoxy	deoxy surrounded[c] by oxy in oxy cell	oxy in[d] oxy	$Fe(O_2)$(TpivPP)-(1-MeIm)[e]
IC(2)-EC(2)	1	3.36		3.30	
IC(2)-EO(1)	1	3.96		3.87	

[a] The symmetry operation applied to the second atom is in ORTEP format (Johnson, C. K. ORNL-5138, 1976). The first three digits specify unit cell translations parallel to *a*, *b*, and *c*, respectively, e.g., 546 denotes no translation along *a*, a translation of −1 along *b*, and +1 along *c*. The last two digits specify the symmetry operation in the order: 01 (x, y, z); 02 $(-x, y, \frac{1}{2} - z)$; 03, $(x, -y, \frac{1}{2} + z)$; 04, $(\frac{1}{2} + x, \frac{1}{2} + y, z)$; 05, $(\frac{1}{2} + x, \frac{1}{2} - y, \frac{1}{2} + z)$; 06, $(-x, -y, -z)$; 07 $(\frac{1}{2} - x, \frac{1}{2} - y, -z)$; 08, $(\frac{1}{2} - x, \frac{1}{2} + y, \frac{1}{2} - z)$. [b] Intermolecular contacts for I. [c] Intermolecular contacts for a molecule of I surrounded by molecules of II. The unit cell for II is used. See footnote 36. [d] Intermolecular contacts for II. [e] Analogous contacts for $Fe(O_2)$(TpivPP)(1-MeIm).

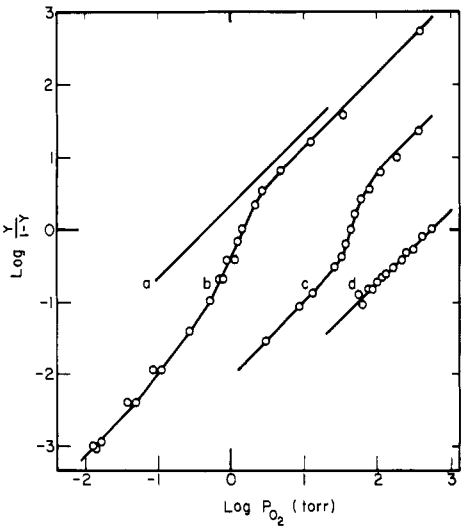

Figure 11. Uptake of dioxygen by (a) solid Fe(TpivPP)(1-MeIm), (b) Fe(TpivPP)(2-MeIm), (c) Fe(TpivPP)(1,2-Me_2Im), and (d) Fe(TpivPP)(2-MeIm)·EtOH.

Table XIX. Cooperativity in O_2 Binding

system	$P_{1/2}$, Torr (25 °C) high affinity "R"	low affinity "T"	Hill coefficient
Fe(TpivPP)(1-MeIm)[a]	0.5 (noncooperative)		1.0
Fe(TpivPP)(2-MeIm)[a]	0.7	14	2.6
Fe(TpivPP)(1,2-Me_2Im)[a]	14	112	3.0
Fe(TpivPP)(1-MeIm)·EtOH[b]	(noncooperative)	620	1.0
HbA, stripped, pH 7.4[c]	0.3	9	2.5

[a] Reference 18. [b] This work. [c] Tyuma, I.; Imai, K.; Shimizu, K. *Biochemistry* **1973**, *12*, 1491-1498. Imai, K.; Yonetani, T.; Ikeda-Saito, M. *J. Mol. Biol.* **1977**, *109*, 83-97.

anthroline)iron(II) and also its α-picoline solvate display a sharp, cooperative transition, whereas the pyridine solvate remains high spin over the entire range of 300 to 80 K.[57a,b] Other examples involving solvates of benzene, chloroform, and water have been reported.[57a,c-f] Structural studies indicate the expected reduction of iron–ligand bond distances upon transition from high to low spin, and this is thought to be the origin of the observed cooperativity.[57a] Although a full explanation of these phenomena is not yet in hand, nucleation and domain growth are central in the evolving theories[58] proposed for the crossover systems. In general terms, these same concepts may be applicable to solid state O_2 binding. In this analogy, our complexes could be viewed as related systems in which O_2 pressure, rather than temperature, is the variable influencing the spin state.

The general trend in dioxygen affinities, seen in Figure 11, can be rationalized in terms of increasing steric restraint to motion of the axial base upon oxygenation. The change from the unhindered 1-MeIm to the hindered 2-MeIm ligand produces a tenfold decrease in dioxygen affinity. Another tenfold decrease occurs on replacing 2-MeIm with 1,2-Me_2Im as the axial base. This is the result of the buttressing interaction of the 1-methyl against the 2-methyl substituent which increases steric contact between the 2-methyl substituent and the porphyrinato skeleton. The even lower affinity observed for I cannot be attributed to reduced access of dioxygen to the binding site—this is a kinetic, not thermodynamic, phenomenon. The diminished affinity of I for dioxygen presumably reflects an increased resistance to motion toward the porphyrinato skeleton by the 2-MeIm moiety together with its hydrogen-bonded ethanol. This is consistent with the apparently decreased occupancy of the hydrogen-bonding site in the oxy form, II. Inspection of Table XVII shows the substantial changes in nonbonded contacts made by the hydrogen-bonded ethanol molecule.

Structural Comparison with Hb and Mb. One intent of studies of synthetic analogues of metalloproteins is to generate information which can serve as a base line for understanding structure and function relationships in proteins. One should not assume that the behavior of model compounds represents that of an active site free of external influence by the protein. In fact, external influences, such as solvation and crystal packing effects, also exist in model compounds. For example, the differences in the structures of Fe(TPP)(2-MeIm)·EtOH and Fe(TpivPP)(2-MeIm)·EtOH, discussed earlier, although small and beyond detection in structural analyses of hemoproteins, are nonetheless significant. Thus, strictly speaking, neither is truly representative of the "free molecule", undistorted by crystal packing influences. However, it is possible to change the conditions responsible for these effects and thus gain some knowledge of the isolated site behavior. Certain caveats must be given in making comparisons between these model systems and the hemoproteins: TpivPP is not protoporphyrin IX; intermolecular solid-state interactions are not intersubunit conformational changes; the hindrance created by the 2-MeIm ligand is not a protein-generated restraint. Nonetheless, the deoxy structure, I, with the sterically demanding 2-MeIm ligand, remains a plausible model for T-state deoxyhemoglobin. The oxy structure, II, should not be compared with R-state oxyhemoglobin: the 2-MeIm ligand of II can never be unrestrained (as are relaxed oxyhemoproteins or $Fe(O_2)$(TpivPP)(1-MeIm)). However, complex II may be a simple analogue of T-state oxyhemoglobin. The Fe-N_{Im} separation is essentially the same for complexes I and II, and also for $Fe(O_2)$(TpivPP)(1-MeIm),[12] consistent with the Mössbauer results of Huynh et al.[37] on isolated hemoglobin chains and T-state deoxyhemoglobin and with the recent resonance Raman results of Kincaid et al.[25c] on R- and T-state deoxy-

Table XX. Stereochemistry of Hemoproteins and Their Model Analogues[a]

complex	M···Ct	M···P_c	M-N_p	M-N_{Im}	M-O	O-O	∠MOO, deg
Fe(TPP)(2-MeIm)·EtOH[b]	0.42	0.55	2.086(4)	2.161(5)			
Fe(TpivPP)(2-MeIm)·EtOH[c]	0.399	0.43	2.072(5)	2.095(6)			
Mb[d]	0.42	0.55	2.06	2.1			
Hb[e] α		0.60(10)	2.1(1)	2.0(3)			
β		0.63(10)	2.1(1)	2.2(3)			
erythrocruorin[f]	0.23	0.17	2.02	2.2			
$Fe(O_2)$(TpivPP)(1-MeIm)[g,h]	−0.02	−0.03	1.98(1)	2.07(2)	1.75(2)	>1.16(4)	<131(2)
$Mb(O_2)$[i]	0.24	0.24	2.07(7)	2.03(7)	2.02(7)	1.21(10)	111
oxycobaltomyoglobin[j]	0.25		1.99(8)	1.97(8)	1.89(8)	1.26(8)	131
oxyerythrocruorin[k]	0.38	0.30	2.04(10)	2.1(2)	1.8(2)	1.25(20)	170(30)
$Fe(O_2)$(TpivPP)(2-MeIm)·EtOH[c,h]	0.086	0.119	1.996(4)	2.107(4)	1.898(7)	>1.22(2)	<129(2)

[a] All distances in Å. Estimated standard deviations, when available, are in parentheses. N_{Im}, coordinated nitrogen atom of the imidazole ligand; P_c, center of mean porphyrinato plane. See Figures 8 and 9 for definition of N_p and Ct. [b] Reference 34. [c] This work. [d] Reference 48; resolution 2.0 Å. [e] References 49 and 50; resolution 2.5 Å. [f] References 51-53; resolution 1.4 Å. [g] Reference 12. [h] Fe-O-O angle and O-O separations affected by disorder. [i] Reference 45 and Phillips, S. E. V., personal communication; resolution 1.6 Å. [j] Reference 46; resolution 1.5 Å. [k] References 47 and 53; resolution 1.4 Å.

hemoglobin. Significantly, it is the Fe-O bond length which is lengthened in II. This is a result of considerable interest since some discussions on cooperativity[9,34] have stressed the significance of assumed changes in the Fe-N_{Im} and Fe···Ct separations upon oxygenation. It has been proposed that it is the Fe-N_{Im} bond which is under "tension" in T-state oxyhemoglobin.[9] Furthermore, in the very recent studies by Budge et al.[38,39] on ligand binding to iron(II) "capped" porphyrins[40] in solution, a porphyrin with a larger "cap" possesses a *lower* affinity for dioxygen. Since the axial base was kept constant, the porphyrin rather than the axial base would appear to be controlling dioxygen affinity in this case. In the solid-state structure of the free-base "H_2Cap" porphyrin, the porphyrin skeleton is highly buckled,[41] a situation likely to occur for iron(II) derivatives of this "capped" porphyrin.

In contrast, long Fe-N_{Im} and short Fe-N_{NO} separations are observed for Fe(NO)(TPP)(1-MeIm).[14] This, and also the observation that in T-state nitrosylhemoglobin there is apparently rupture of the Fe-N_{Im} bond,[42-44] reflects the stronger affinity of an Fe(porphyrinato)(imidazole) complex for NO compared with O_2 and the different trans-labilizing properties of these ligands.

Recently, preliminary reports of the structures of oxymyoglobin, oxycobaltomyoglobin, and oxyerythrocruorin have appeared.[45-47] Relevant bond parameters for these and other hemoproteins[48-53] and their synthetic analogues are included in Table XX. For oxymyoglobin[45] the Fe-O-O unit is, reassuringly, bent as observed for the "picket-fence" porphyrin complexes. But for oxyerythrocruorin,[47] the very large error (30°) associated with the apparently near-linear Fe-O-O bond angle of 170° should preclude any definitive conclusion. For oxycobaltomyoglobin,[46] hydrogen bonding between the *coordinated* oxygen atom and the distal histidine is postulated; the Co-O-O geometry is bent and similar to that for $Mb(O_2)$ and cobalt-Schiff base dioxygen complexes.[54]

Unexpectedly large displacements of the iron atom from the porphyrinato plane toward the coordinated histidine residue are observed for both $Mb(O_2)$[45] and oxyerythrocruorin[47] (see Table XX). For these proteins this may result from the eclipsed orientation of the imidazole plane relative to the Fe-N_p bonds, which does not occur for $Fe(O_2)$(TpivPP)(1-MeIm) or II. Upon oxygenation of Mb the iron atom moves ~0.3 Å toward the porphyrin plane, whereas in erythrocruorin the iron atom appears to move even further out of the plane (by ~0.1 Å). For oxycobaltomyoglobin the cobalt atom is 0.25 Å from the plane of the porphyrinato nitrogen atoms, whereas for the model compounds[2,55] for deoxycobaltomyoglobin, Co(porphyrin)(1-MeIm), the displacement is 0.13-0 16 Å.[56] Whether one perceives significant differences in these metrical comparisons of proteins and models is very much a function of the faith one puts in those standard deviations estimated on occasion in the protein studies.

In the solid state and in the hemoproteins, oxygen affinity should be sensitive to the orientation of the axial base. A lower affinity is likely when the axial base is in the eclipsing ($\phi = 0°$) rather than the bisecting conformation ($\phi = 45°$). The latter conformation probably occurs for model compounds in solution where the steric constraints of crystal packing or of a protein envelope are absent. It has been generally assumed that the structures of myoglobin in single crystals and in solution are identical, at least in the immediate environment of the heme. One could test this assumption by comparing the dioxygen affinities of Mb in solution and in single crystals. It is possible that a more nearly eclipsing conformation for the histidine ligand in low-affinity T-state hemoglobin relative to high-affinity R-state hemoglobin may be a significant factor in the cooperative binding of small molecules by hemoglobin.

Acknowledgments. This work was supported at Northwestern University by the National Institutes of Health (HL-13157) and at Stanford University by the National Institutes of Health (GM-17880) and the National Science Foundation (CHE-75-17018). We thank the Hertz Foundation (K.S.S.) and the North Atlantic Treaty Organization (E.R.) for fellowship support.

Supplementary Material Available: Idealized hydrogen positions (Tables IV and VIII), observed and calculated structure amplitudes (Tables V and IX), metrical changes on oxygenation (Table XIII), least-squares planes (Table XIV), dihedral angles between planes (Table XV), nonbonded contacts (Table XVI), and intermolecular hydrogen contacts (Table XVIII) (44 pages). Ordering information is given on any current masthead page.

References and Notes

(1) (a) Northwestern University. (b) Stanford University. (c) University of Illinois.
(2) (a) Ibers, J. A.; Lauher, J. W.; Little, R. G. *Acta Crystallogr., Sect. B* **1974**, *30*, 268-272. (b) Little, R. G.; Ibers, J. A. *J. Am. Chem. Soc.* **1974**, *96*, 4452-4463.
(3) Basolo, F.; Hoffman, B. M.; Ibers, J. A. *Acc. Chem. Res.* **1975**, *8*, 384-392.
(4) (a) Collman, J. P. *Acc. Chem. Res.* **1977**, *10*, 265-272. (b) Collman, J. P.; Brauman, J. I.; Doxsee, K. M.; Halbert, T. R.; Suslick, K. S. *Proc. Natl. Acad. Sci. U.S.A.* **1978**, *75*, 564-568.
(5) (a) Collman, J. P.; Halbert, T. R.; Suslick, K. S. In "O_2 Binding and Activation by Metal Centers", Spiro, T. G., Ed.; Wiley: New York, 1980. (b) Jones, R. D.; Summerville, D. A.; Basolo, F. *Chem. Rev.* **1979**, *79*, 139-178. (c) Reed, C. A. In "Metal Ions in Biological Systems", Sigel, H., Ed.; Marcel Dekker: New York, 1978; pp 278-310. (d) Traylor, T. G. In "Bioorganic Chemistry", van Tamelen, E. E., Ed.; Academic Press: New York, 1978; Chapter 4. (e) Buchler, J. W. *Angew. Chem., Int. Ed. Engl.* **1978**, *17*, 407-423. (f) James, B. In "The Porphyrins", Dolphin, D., Ed.; Academic Press: New York, 1978; Chapter 5. (g) Vaska, L. *Acc. Chem. Res.* **1976**, *9*, 175-183. (h) Erskine, R. W.; Field, B. O. *Struct. Bonding (Berlin)* **1976**, *28*, 3-50.

(6) Eisenberger, P.; Shulman, R. G.; Kincaid, B. M.; Brown, G. S.; Ogawa, S. *Nature (London)* **1978,** *274,* 30–34.
(7) Warshel, A. *Proc. Natl. Acad. Sci. U.S.A.* **1977,** *74,* 1789–1793.
(8) Gelin, B. R.; Karplus, M. *Proc. Natl. Acad. Sci. U.S.A.* **1977,** *74,* 801–805.
(9) (a) Perutz, M. F. *Nature (London)* **1970,** *228,* 726–739. (b) *Ibid.* **1972,** *237,* 495–499.
(10) (a) Perutz, M. F. *Br. Med. Bull.* **1976,** *32,* 195–208. (b) *Sci. Am.* **1978,** *239*(6), 92–125.
(11) Collman, J. P.; Gagne, R. R.; Reed, C. A.; Robinson, W. T.; Rodley, G. A. *Proc. Natl. Acad. Sci. U.S.A.* **1974,** *71,* 1326–1330.
(12) Jameson, G. B.; Rodley, G. A.; Robinson, W. T.; Gagne, R. R.; Reed, C. A.; Collman, J. P. *Inorg. Chem.* **1978,** *17,* 850–857.
(13) Peng, S.-M.; Ibers, J. A. *J. Am. Chem. Soc.* **1976,** *98,* 8032–8036.
(14) Scheidt, W. R.; Piciulo, P. L. *J. Am. Chem. Soc.* **1976,** *98,* 1913–1919.
(15) Jameson, G. B.; Ibers, J. A. *Inorg. Chem.* **1979,** *18,* 1200–1208.
(16) Abbreviations: TPP, *meso*-tetraphenylporphyrinato; TpivPP, *meso*-tetra($\alpha,\alpha,\alpha,\alpha$-*o*-pivalamidephenyl)porphyrinato; 1-MeIm, 1-methylimidazole; 2-MeIm, 2-methylimidazole; 1,2-Me_2Im, 1,2-dimethylimidazole; Hb, hemoglobin A; Mb, sperm whale myoglobin; EtOH, ethanol.
(17) See, for example, Bunn, H. F.; Forget, B. G.; Ranney, H. M. "Human Hemoglobins"; W. B. Saunders: Philadelphia, 1977.
(18) Collman, J. P.; Brauman, J. I.; Rose, E.; Suslick, K. S. *Proc. Natl. Acad. Sci. U.S.A.* **1978,** *75,* 1052–1055.
(19) Rougee, M.; Brault, D. *Biochemistry* **1975,** *14,* 4100–4106.
(20) (a) Geibel, J.; Cannon, J.; Campbell, D.; Traylor, T. G. *J. Am. Chem. Soc.* **1978,** *100,* 3575–3985. (b) White, D. K.; Cannon, J. B.; Traylor, T. G. *Ibid.* **1979,** *101,* 2443–2454.
(21) Although it is implicitly assumed[20] that the conformation of the porphyrin skeleton is unaffected by the nature of the covalent linkage between imidazole and porphyrin, we would expect that at least some of the steric strain so induced in the Fe–N_{Im} bond would be dissipated by conformational changes in the porphyrin skeleton.
(22) Marchant, L.; Sharrock, M.; Hoffman, B. M.; Munck, E. *Proc. Natl. Acad. Sci. U.S.A.* **1972,** *69,* 2396–2399.
(23) Spartalian, K.; Lang, G.; Collman, J. P.; Gagne, R. R.; Reed, C. A. *J. Chem. Phys.* **1975,** *63,* 5375–5382.
(24) Lang, G.; Marshall, W. *Proc. Phys. Soc., London* **1966,** *87,* 3–34.
(25) (a) Burke, J. M.; Kincaid, J. R.; Peters, S.; Gagne, R. R.; Collman, J. P.; Spiro, T. G. *J. Am. Chem. Soc.* **1978,** *100,* 6083–6088. (b) Spiro, T. G.; Burke, J. M. *Ibid.* **1976,** *98,* 5482–5489. (c) Kincaid, J.; Stein, P.; Spiro, T. G. *Proc. Natl. Acad. Sci. U.S.A.* **1979,** *76,* 549–552. Correction: *Ibid.* **1979,** *76,* 4156.
(26) Brunner, H. *Naturwissenschaften* **1974,** *61,* 129.
(27) Maxwell, J. C.; Caughey, W. S. *Biochem. Biophys. Res. Commun.* **1974,** *60,* 1309–1314.
(28) Jones, R. D.; Budge, J. R.; Ellis, P. E. Jr.; Linard, J. E.; Summerville, D. A.; Basolo, F. *J. Organomet. Chem.* **1979,** *181,* 151–158.
(29) Jameson, G. B.; Molinaro, F. S.; Ibers, J. A.; Collman, J. P.; Brauman, J. I.; Rose, E.; Suslick, K. S. *J. Am. Chem. Soc.* **1978,** *100,* 6769–6770.
(30) For example, Waters, J. M.; Ibers, J. A. *Inorg. Chem.* **1977,** *16,* 3273–3277.
(31) See paragraph at end of paper regarding supplementary material.
(32) Collman, J. P.; Brauman, J. I.; Doxsee, K. M.; Halbert, T. R.; Hayes, S. E.; Suslick, K. S. *J. Am. Chem. Soc.* **1978,** *100,* 2761–2766.
(33) Jameson, G. B.; Robinson, W. T.; Collman, J. P.; Sorrell, T. N. *Inorg. Chem.* **1978,** *17,* 858–864.
(34) Hoard, J. L. In "Porphyrins and Metalloporphyrins", Smith, K. M., Ed.; Elsevier: Amsterdam, 1975; pp 317–380.
(35) Kirner, J. F.; Reed, C. A.; Scheidt, W. R. *J. Am. Chem. Soc.* **1977,** *99,* 2557–2563.
(36) Changes in unit cell dimensions are sufficiently small that the simple difference in fractional coordinations between I and II suffices for the calculation of atom movements.
(37) Huynh, B. H.; Papaefthymiou, G. C.; Groves, J. L.; Wu, C. S. *Biochem. Biophys. Res. Commun.* **1974,** *60,* 1295–1301.
(38) Budge, J. R.; Ellis, Jr., P. E.; Jones, R. D.; Linard, J. E.; Szymanski, T.; Basolo, F.; Baldwin, J. E.; Dyer, R. L. *J. Am. Chem. Soc.* **1979,** *101,* 4762–4763.
(39) Budge, J. R.; Ellis, Jr., P. E.; Jones, R. D.; Linard, J. E.; Basolo, F.; Baldwin, J. E.; Dyer, R. L. *J. Am. Chem. Soc.* **1979,** *101,* 4760–4762.
(40) (a) Almog, J.; Baldwin, J. E.; Dyer, R. L.; Peters, M. *J. Am. Chem. Soc.* **1975,** *97,* 226–227. (b) Almog, J.; Baldwin, J. E.; Huff, J. *Ibid.* **1975,** *97,* 227–228.
(41) Jameson, G. B.; Ibers, J. A. *J. Am. Chem. Soc.*, in press.
(42) Perutz, M. F.; Kilmartin, J. V.; Nagai, K.; Szabo, A.; Simon, S. R. *Biochemistry* **1976,** *15,* 378–387.
(43) Maxwell, J. C.; Caughey, W. S. *Biochemistry* **1976,** *15,* 388–396.
(44) It has been suggested (Chevion, M.; Salhany, J. M.; Peisach, J.; Castillo, C. L.; Blumberg, W. E. *Isr. J. Chem.* **1977,** *15,* 311–317) that the ESR results of Maxwell and Caughey[43] were on denatured nitrosylhemoglobin. The former propose that the proximal histidine remains coordinated in both R- and T-state nitrosylhemoglobin, although the proximal histidine proton at position N(1) of the chains disappears in the transition from T- to R-state hemoglobin with a consequent change in the N_{NO} superhyperfine structure.
(45) Phillips, S. E. V. *Nature (London)* **1978,** *273,* 247–248.
(46) Petsko, G. A.; Rose, D.; Tsernoghon, D.; Ikeda-Saito, M.; Yonetani, T. *J. Biol. Chem.*, in press.
(47) Weber, E.; Steigemann, W.; Jones, T. A.; Huber, R. *J. Mol. Biol.* **1978,** *120,* 327–336.
(48) Takano, T. *J. Mol. Biol.* **1977,** *110,* 569–584.
(49) Fermi, G. *J. Mol. Biol.* **1975,** *97,* 237–256.
(50) Ten Eyck, L. F.; Arnone, A. *J. Mol. Biol.* **1976,** *100,* 3–11.
(51) Huber, R.; Epp, O.; Formanek, H. *J. Mol. Biol.* **1970,** *52,* 349–354.
(52) Huber, R.; Epp, O.; Steigemann, W.; Formanek, H. *Eur. J. Biochem.* **1971,** *19,* 42–50.
(53) Steigemann, W.; Weber, E. *J. Mol. Biol.*, in press.
(54) For example, Rodley, G. A.; Robinson, W. T. *Nature (London)* **1972,** *235,* 438–439. Gall, R. S.; Schaefer, W. P. *Inorg. Chem.* **1976,** *15,* 2758–2763.
(55) Scheidt, W. R. *J. Am. Chem. Soc.* **1974,** *96,* 90–94.
(56) In the report of the structure of *meso*-porphyrinato IX cobalt(II) myoglobin (Padlan, E. A.; Eaton, W. A.; Yonetani, T. *J. Biol. Chem.* **1975,** *250,* 7069–7073) no mention was made of the out-of-plane displacement of the cobalt atom.
(57) (a) Goodwin, H. A. *Coord. Chem. Rev.* **1976,** *18,* 293–325. (b) König, E.; Ritter, G.; Madeja, K.; Bohmer, W. H. *Ber. Bunsenges. Phys. Chem.* **1973,** *77,* 390–398. (c) Sylva, R. N.; Goodwin, H. A. *Aust. J. Chem.* **1968,** *21,* 1081–1084. (d) König, E.; Ritter, G.; Goodwin, H. A. *Chem. Phys.* **1974,** *5,* 211–223. (e) Sylva, R. N.; Goodwin, H. A. *Aust. J. Chem.* **1967,** *20,* 479–496. (f) Dosser, R. J.; Eilbeck, W. J.; Underhill, A. E.; Edwards, P. R.; Johnson, C. E. *J. Chem. Soc. A* **1969,** 810–816.
(58) (a) Sorai, M.; Seki, S. *J. Phys. Chem. Solids* **1974,** *35,* 555–570. (b) Gutlich, P.; Köppen, H.; Link, R.; Steinhause, H. G. *J. Chem. Phys.* **1979,** *70,* 3977–3983. (c) Rao, C. N. R.; Rao, K. J. "Phase Transitions in Solids"; McGraw-Hill: New York, 1978. (d) Haddad, M. S.; Federer, W. D.; Lynch, M. W.; Hendrickson, D. N. *J. Am. Chem. Soc.* **1980,** *102,* 1468–1470.